# Coherent chaos in a recurrent neural network with structured connectivity

Itamar Daniel Landau[1] and Haim Sompolinsky[1,2]

[1]Edmond and Lily Safra Center for Brain Sciences, The Hebrew University of Jerusalem, Jerusalem, Israel

[2]Center for Brain Science, Harvard University, Cambridge, MA, USA

**Abstract**

We present a simple model for coherent, spatially correlated chaos in a recurrent neural network. Networks of randomly connected neurons exhibit chaotic fluctuations and have been studied as a model for capturing the temporal variability of cortical activity. The dynamics generated by such networks, however, are spatially uncorrelated and do not generate coherent fluctuations, which are commonly observed across spatial scales of the neocortex. In our model we introduce a structured component of connectivity, in addition to random connections, which effectively embeds a feedforward structure via unidirectional coupling between a pair of orthogonal modes. Local fluctuations driven by the random connectivity are summed by an output mode and drive coherent activity along an input mode. The orthogonality between input and output mode preserves chaotic fluctuations even as coherence develops. In the regime of weak structured connectivity we apply a perturbative approach to solve the dynamic mean-field equations, showing that in this regime coherent fluctuations are driven passively by the chaos of local residual fluctuations. Strikingly, the chaotic dynamics are not subdued by even very strong structured connectivity if we add a row balance constraint on the random connectivity. In this regime the system displays longer time-scales and with switching-like activity reminiscent of "Up-Down" states observed in cortical circuits. The level of coherence grows with increasing strength of structured connectivity until the dynamics are almost entirely constrained to a single spatial mode. We describe how in this regime the model achieves intermittent self-organized criticality in which the coherent component of the dynamics self-adjusts to yield periods of slow chaos. Furthermore, we show how the dynamics depend qualitatively on the particular realization of the connectivity matrix: a complex leading eigenvalue can yield coherent oscillatory chaotic fluctuations while a real leading eigenvalue can yield chaos with broken symmetry. We examine the effects of network-size scaling and show that these results are not finite-size effects. Finally, we show that in the regime of weak structured connectivity, coherent chaos emerges also for a generalized structured connectivity with multiple input-output modes.

## Author Summary

Neural activity observed in the neocortex is temporally variable, displaying irregular temporal fluctuations at every accessible level of measurement. Yet these temporal fluctuations are often found to be spatially correlated whether at the scale of local measurements such as membrane potentials and spikes, or global measurements such as EEG and fMRI. A thriving field of study has developed models of recurrent networks which intrinsically generate irregular temporal variability, the paradigmatic example being networks of randomly connected rate neurons which exhibit chaotic dynamics. These models have been examined analytically and numerically in great detail, yet until now the intrinsic variability generated by these networks have been spatially uncorrelated, yielding no large-scale coherent fluctuations. Here we present a simple model of a recurrent network of firing-rate neurons that intrinsically generates spatially correlated activity yielding coherent fluctuations across the entire network. The model incorporates random connections and adds a structured component of connectivity that sums network activity over a spatial "output" mode and projects it back to the network along an orthogonal "input" mode. We show that this form of structured

connectivity is a general mechanism for producing coherent chaos.

## Introduction

Firing-rate fluctuations and irregular spiking are ubiquitous in the neocortex[28, 3]. Furthermore this temporal variability is often observed to be correlated across spatial scales ranging from local cortical circuits to the entire brain: in local cortical circuits both in membrane potential fluctuations [40] and on the level of spiking [27, 4, 20, 21], in the coherency measured in brain-wide EEG signals [19, 1], and in the global signal observed across all voxels in fMRI measurements [26, 14, 18].

A class of theoretical models has successfully accounted for temporal variability via internally generated chaotic dynamics of recurrent networks, whether through excitation-inhibition balance in spiking models[38, 23] or the more abstract models of rate chaos in randomly connected networks[30]. Yet a key emergent feature of these models is the decorrelation of neural activity such that the macroscopic, population activity remains nearly constant in time. Population-wide coherence or synchrony can be generated in a variety of ways for example by introducing spatial modes with self-excitation, but this comes at a cost of drowning out the chaotic fluctuations and yielding fixed points [35]. Indeed a major challenge to theorists has been to produce network models which generate spatially coherent, temporally irregular fluctuations which can account for broad spatial correlations observed in experiments.

Two recent studies have shown that excitation-inhibition balance networks can generate spatially modulated correlations [25, 6]. In both of these studies the correlations are driven by common input from an external source, and the average correlation across the network remains small. It remains an open question whether a network can internally generate correlated fluctuations that are coherent across the entire network.

The chaotic dynamics of a network of randomly connected firing-rate neurons has been well-studied [30, 12]. In such a network each individual neuron's firing rate is given by a non-linear function of its input, which is in turn a weighted sum of the firing rates of all other neurons in the network. The network exhibits a phase transition from a fixed point to chaotic activity in which the randomness of the weights reverberates uncorrelated fluctuations throughout the network. Typically in this chaotic regime pairwise correlations are small and no coherent fluctuations emerge. Here we extend this model by adding a low-rank structured component of connectivity to the random connections. The structured connectivity sums the fluctuations along one spatial mode and projects them along a second, orthogonal mode yielding coherent fluctuations without drowning out the individual neuron variability which continues to drive the chaotic dynamics. A previous work studied a specific example of this structure and focused primarily on analyzing the non-chaotic regime[8]. Here we focus on the chaotic regime and show that

this form of structured connectivity together with random connections provides a basic mechanism for internally generating coherent fluctuations.

# Results

We study a network of $N$ neurons in which the connectivity between neurons has two components: a random component, $\mathbf{J}$, and a rank-1 structured component, $\mathbf{M} = \frac{J_1}{\sqrt{N}}\boldsymbol{\xi}\boldsymbol{\nu}^T$ , an outer product of a pair of orthogonal vectors both of which have elements of $O(1)$ and norm $\sqrt{N}$, with strength parameter $J_1$. We restrict the elements of $\boldsymbol{\xi}$ to be binary, $\xi_i = \pm 1$, which will be important for some of the results to come, and we will comment on when this restriction can be relaxed. We can think of the row vector, $\boldsymbol{\nu}^T$, as an "output mode" performing a read-out of the network activity, and the column vector, $\boldsymbol{\xi}$, as a corresponding "input mode" along which the output mode activity is fed back to the network. (Fig 1A) .

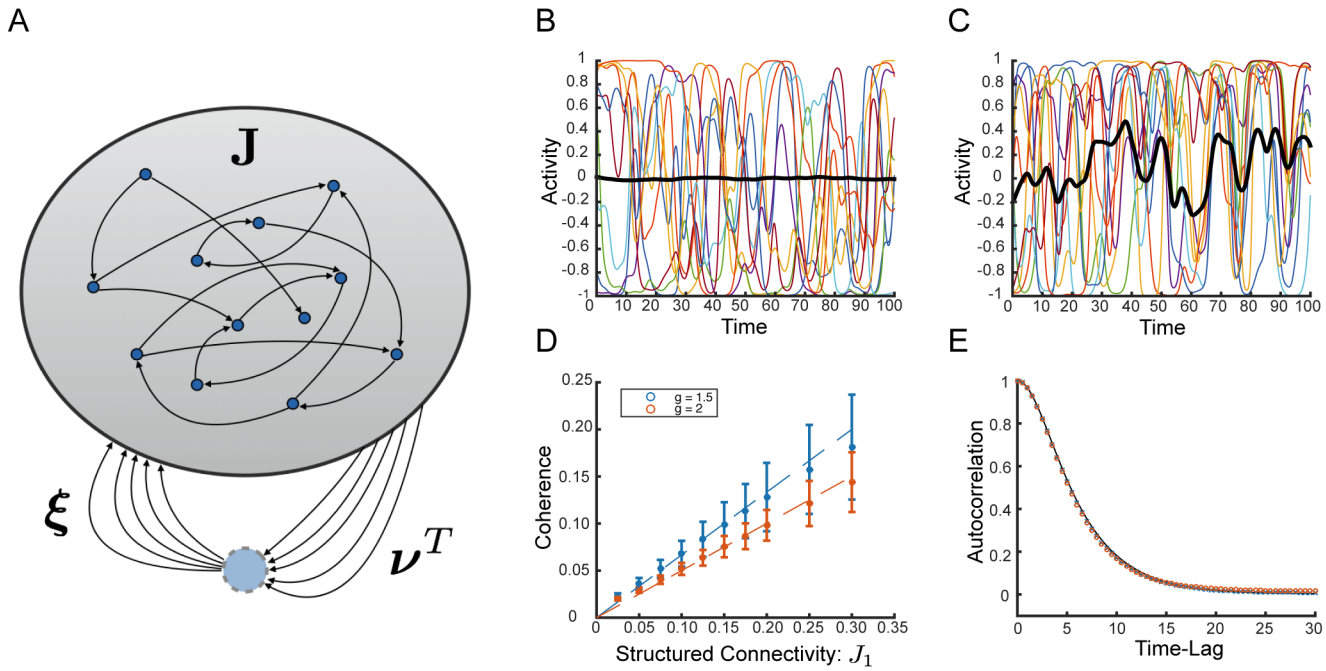


**Figure 1. Weak Structured Connectivity Generates Passive Coherence.** **(A)** Network schematics showing neurons connected via random matrix $\mathbf{J}$ and rank-one structured connectivity. The structured component is represented schematically as a feed-forward loop with drive through the output mode, $\boldsymbol{\nu}$, and feedback through the input mode, $\boldsymbol{\xi}$. The standard deviation of the random component is given by $\frac{g}{\sqrt{N}}$ and the strength of the structured component is $\frac{J_1}{\sqrt{N}}$. **(B)** Sample network dynamics without structured component, i.e. $J_1 = 0$, colored traces show a random collection of ten neural activity patterns, $\phi_j$, black trace shows the coherent mode activity, $\bar{\phi} = \frac{1}{N}\sum_j \xi_j \phi_j$. **(C)** Sample dynamics for $J_1 = 1$. Coherent mode displays substantial fluctuations. **(D)** Coherence $\chi$ (Expression in Text), as a function of the strength of structured connectivity component, $J_1$. Simulation and theory shown for both $g = 1.5$ and $g = 2$. Bars show standard deviation over 60 realization of the random connectivity. **(E)** Normalized autocorrelation of the coherent component of the current in red circles. Average normalized autocorrelation of the residuals in blue 'x's. Both are averaged over 60 realizations of the random connectivity with $J_1 = 0.1$. Prediction from theory in black. $N = 4000$ and $g = 2$ in all panels unless stated otherwise.

The random component of the connectivity is given by the matrix $\mathbf{J}$ consisting of identically distributed independent Gaussian elements with mean 0 and variance $\frac{g^2}{N}$, where $g$ is an $O(1)$ parameter.

The state of each neuron is defined by its synaptic current, $h_i(t)$, with its firing rate given by $\phi_i \equiv \phi(h_i(t))$, where $\phi$ is a sigmoidal function. For some later results it will be necessary to assume that $\phi$ has a first derivative that is an even function. We therefore assume here for concreteness $\phi(h) = \tanh(h)$ unless otherwise noted, and we comment on when this assumption can be relaxed.

The dynamics of the synaptic current vector, $\mathbf{h}$, is given by

$$\frac{\mathrm{d}\mathbf{h}}{\mathrm{d}t} = -\mathbf{h} + \mathbf{J}\boldsymbol{\phi} + \frac{J_1}{\sqrt{N}}\boldsymbol{\xi}\boldsymbol{\nu}^T\boldsymbol{\phi} \tag{1}$$

We have scaled the strength of the structured connectivity such that when the scaling-parameter $J_1 \sim O(1)$ the contribution of the structure to individual synapses is of the same order of magnitude as the typical random connection.

We will be particularly interested in the coherent activity and the coherent current, i.e. the spatial overlap of both the firing rate and the synaptic current with the input mode. These are defined respectively as

$$\bar{\phi} \equiv \frac{1}{N}\sum_j \xi_j \phi_j,\ \bar{h} \equiv \frac{1}{N}\sum_j \xi_j h_j, \tag{2}$$

We define the measure of coherence as the fraction of the total standard deviation of the network current $h_i$ that is shared along the coherent mode, $\bar{h}$:

$$\chi \equiv \sqrt{\frac{\langle \bar{h}^2 \rangle}{\frac{1}{N}\sum_i \langle h_i^2 \rangle}} \tag{3}$$

where $\langle\ \rangle$ represents average over time. This is a useful measure as it varies from 0 to 1, and will yield $\chi = 1/\sqrt{N}$ for entirely independent, uncoupled fluctuations, and $\chi = 1$ for complete synchrony along $\boldsymbol{\xi}$.

Without the structured component, i.e. $J_1 = 0$, the network exhibits a phase transition at $g = 1$ from a zero fixed point to chaos[30]. In the chaotic state the randomness of the connectivity decorrelates the input current and yields an asynchronous state in which neurons fluctuate with negligible correlations such that both $\bar{\phi}$ and $\bar{h}$ are nearly constant in time, and $\chi \approx \frac{1}{\sqrt{N}}$ (Fig 1B).

Setting $J_1 = 1$, we observe significant correlations along the input mode, such that the coherent mode activity, $\bar{\phi}$, fluctuates significantly. For this network with $N = 4000$ we find the coherence $\chi \approx 0.4$, which is about 25 times larger than is observed in the asynchronous state. (Fig 1C).

In order to analyze this system we decompose the dynamics of the synaptic currents into coherent component, $\bar{h}$, and the vector of residuals currents, $\delta\mathbf{h} = \mathbf{h} - \bar{h}\boldsymbol{\xi}$. We also decompose the activity into its coherent component, $\bar{\phi}$, and vector of residual activity, $\delta\boldsymbol{\phi} = \boldsymbol{\phi} - \bar{\phi}\boldsymbol{\xi}$. Because of the orthogonality between input and output mode, the output mode ignores the coherent component, $\bar{\phi}$, and projects only the activity of the residuals: $\boldsymbol{\nu}^T\boldsymbol{\phi} = \boldsymbol{\nu}^T\delta\boldsymbol{\phi}$.

By averaging the dynamic equations 1 over the input mode, $\boldsymbol{\xi}$, we can write decomposed dynamics for the residual synaptic currents and for the coherent current:

$$\frac{\mathrm{d}\delta\mathbf{h}}{\mathrm{d}t} = -\delta\mathbf{h} + \hat{\mathbf{J}}\boldsymbol{\phi} \tag{4}$$

$$\frac{\mathrm{d}\bar{h}}{\mathrm{d}t} \approx -\bar{h} + \frac{J_1}{\sqrt{N}}\boldsymbol{\nu}^T\delta\boldsymbol{\phi} \tag{5}$$

As we discuss more fully in Methods, the effective connectivity matrix in the residual dynamics is

$$\hat{\mathbf{J}} \equiv \left(\mathbf{I} - \frac{\boldsymbol{\xi}\boldsymbol{\xi}^T}{N}\right)\mathbf{J} \tag{6}$$

which projects the output of $\mathbf{J}$ into the $(N-1)$ dimensional subspace orthogonal to $\boldsymbol{\xi}$. This guarantees that the decomposed dynamics satisfy the constraint $\sum_j \xi_j \delta h_j = 0$. For most of what follows this constraint can be ignored as it contributes only $O\left(\frac{1}{\sqrt{N}}\right)$ to each synaptic current. Nevertheless it plays a role later and we introduce it here for completeness. We have, however, ignored the small projection of the random connectivity along the coherent mode ($\frac{\boldsymbol{\xi}^T}{N}\mathbf{J}\boldsymbol{\phi} \sim O\left(\frac{1}{\sqrt{N}}\right)$). Note that even in this approximation, the nonlinearity of $\phi$ in these equations couples the coherent and residual degrees of freedom.

In order to attempt to solve the approximate system we could assume that $\bar{h}(t)$ fluctuates according to some known random process and then consider the dynamics of the $\delta h_i$ with the firing rate of individual units as given by $\phi\left(\delta h_i(t) + \xi_i \bar{h}(t)\right)$. However, for general $J_1$ we are unable to analytically close the loop and self-consistently compute the statistics of $\bar{h}(t)$.

## Mildly Coherent Chaos

In order to proceed analytically, we take a perturbative approach, assuming $J_1 \ll 1$. We turn to computing the autocorrelations of both the coherent component

$$\bar{\Delta}(\tau) \equiv \left\langle \bar{h}(t)\,\bar{h}(t+\tau)\right\rangle \tag{7}$$

and of the residuals,

$$\Delta_\delta(\tau) \equiv \left\langle \delta h_i(t)\,\delta h_i(t+\tau)\right\rangle \ . \tag{8}$$

For small $J_1$ we assume that the coherent current is small ($\bar{h} \ll 1$) and therefore in the dynamics of the residual currents (Eqn 4) we approximate $\phi_i \approx \phi(\delta h_i)$. The result is that to leading order the autocorrelation of the residuals is given by the zeroth-order ($J_1 = 0$) autocorrelation. That is, the residual currents fluctuate as independent Gaussian processes almost identically to the situation without structured connectivity. These residual fluctuations are summed over the output mode yielding substantial fluctuations in $\boldsymbol{\nu}^T\delta\boldsymbol{\phi}$ (recall, $\nu_i \sim O(1)$). These in turn drive the coherent mode and we show in Methods its autocorrelation is given to first-order by

$$\bar{\Delta}(\tau) \approx \left(\frac{J_1}{g}\right)^2 \Delta_\delta(\tau) \tag{9}$$

That is, to leading order the autocorrelation of the coherent component is simply a scaled version of the local, residual autocorrelation.

We verify this prediction numerically in Fig 1E for $J_1 = 0.1$ showing the normalized autocorrelations, $q_{\bar{h}}(\tau) = \frac{\bar{\Delta}(\tau)}{\bar{\Delta}(0)}$ and $q_\delta(\tau) = \frac{\Delta_\delta(\tau)}{\Delta_\delta(0)}$ as well as the prediction from theory. Qualitatively this means that in this regime chaos is driven by the emergent fluctuations in the local synaptic current similar to in the $J_1 = 0$ case, and that the coherent component can be said to absorb these fluctuations passively along the input mode, $\boldsymbol{\xi}$.

In this regime then, the coherence is given simply by

$$\chi = \sqrt{\frac{\bar{\Delta}(0)}{\bar{\Delta}(0) + \Delta_\delta(0)}} \approx \frac{J_1}{g} \tag{10}$$

Numerically, we find that this approximation provides a good description of the system's state for up to $J_1/g = 0.1$ (Fig 1D).

We can understand the coherent chaos in this regime qualitatively: the residual synaptic currents driven by the random connectivity fluctuate as uncorrelated Gaussian processes, and the resulting independent fluctuations in firing rates will be summed over the output mode, $\boldsymbol{\nu}$, which projects to the input mode, $\boldsymbol{\xi}$, driving coherent fluctuations in $\bar{h}(t)$. If the two modes, $\boldsymbol{\xi}$ and $\boldsymbol{\nu}$ had substantial overlap then the coherent fluctuations along $\boldsymbol{\xi}$ would drive positive feedback through $\boldsymbol{\nu}$ driving the neurons to a fixed point. The orthogonality of these modes effectively embeds a feedforward structure from the output mode, $\boldsymbol{\nu}$, to the input mode, $\boldsymbol{\xi}$, within the recurrent connectivity. This enables the persistence of stable fluctuations along the input mode, $\boldsymbol{\xi}$, which do not feedback to $\boldsymbol{\nu}$, thus preventing either saturation or oscillations.

We note that in the regime of mild coherence we can relax the restrictions on $\boldsymbol{\xi}$ and $\phi$: Our results here hold for any $\boldsymbol{\xi}$ which is norm $\sqrt{N}$ and orthogonal to $\boldsymbol{\nu}$, and for any smooth non-linearity.

## "Row Balance" Connectivity

We observe that as $J_1$ increases to values of $O(1)$, the network displays significant variability in the dynamics from realization to realization. The coherent mode autocorrelation function, $\bar{\Delta}(\tau)$, for example, is no longer self-averaging (Fig 2A). We find that the coherent mode variance, given by $\bar{\Delta}(0)$, saturates with increasing system size (Fig 2B).

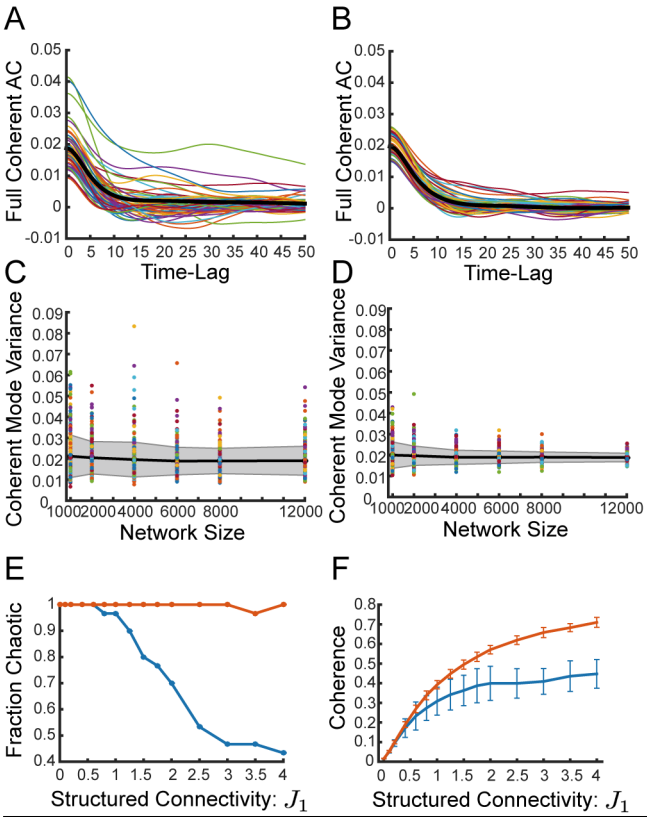


**Figure 2. Row Balance Enables Self-Averaging, Preserves Chaos, and Increases Coherence. (A)-(B)** Full coherent mode autocorrelation, $\bar{\Delta}(\tau)$, of 60 individual realizations, $J_1 = 0.2$ and $N = 4000$. Thick black line shows average over realizations. **(A)** Network with random connectivity $\mathbf{J}$ without row balance. Significant difference between realizations **(B)** Network with "row balance" random connectivity, $\tilde{\mathbf{J}} = \mathbf{J} - \mathbf{J} \cdot \frac{1}{N}\left(\boldsymbol{\xi} \cdot \boldsymbol{\xi}^T\right)$. Individual realizations are all very close to the average. **(C)-(D)** Coherent mode variance, $\bar{\Delta}(0)$, as a function of network size for 300 individual realizations. Black line shows average and gray region shows standard deviation over realizations. **(C)** Without row balance standard deviation saturates. Variability between realizations is not a finite-size effect. **(D)** With row balance standard deviation shrinks, variability between realizations is a finite-size effect. **(E)** Fraction of realizations chaotic as a function of structural connectivity, $J_1$. Row balance keeps nearly all realizations chaotic. **(F)** Coherence, $\chi$, as a function of $J_1$. Row balance increases coherence. $N = 4000$, 30 realizations, red with row balance, blue without for both (E)-(F).

As $J_1$ increases and the fluctuations in the coherent mode grow feedback is generated through the interaction between the random connectivity, $\mathbf{J}$, and the input and output modes, $\boldsymbol{\xi}$ and $\boldsymbol{\nu}$. First of all, $\mathbf{J}$ maps the coherent activity back along the input mode with a small realization-dependent component which we ignored in Eqn 5 such that the coherent activity, $\bar{\phi}$,drives feedback directly to the coherent current, $\bar{h}$. Secondly, $\mathbf{J}$ maps the coherent activity along the the residuals in a realization-dependent direction so that $\bar{\phi}$ biases the residual fluctuations $\delta\mathbf{h}$ along some direction. This direction will have realization-dependent component along the output mode, $\boldsymbol{\nu}$, and therefore the coherent activity may additionally drive feedback by pushing the residual fluctuations along the output mode. See Methods for more details.

To suppress the strong realization dependence of the dynamics, we refine the random connectivity matrix by defining

$$\tilde{\mathbf{J}} \equiv \mathbf{J} - \mathbf{J}\frac{1}{N}\left(\boldsymbol{\xi}\boldsymbol{\xi}^T\right) \tag{11}$$

This subtracts from each row of $\mathbf{J}$ its weighted average along the input mode. This "row balance" subtraction has been previously observed to remove realization-dependent outliers from the eigenspectrum of the full connectivity matrix [22, 34].

We find here that row balance suppresses realization-to-realization variability in the nonlinear chaotic dynamics, for example reducing the variability in the autocorrelation of the coherent mode, $\bar{\Delta}(\tau)$ (Fig 2B). We observe that with row balance this variability drops as a function of increasing system size, suggesting that the dynamics are now self-averaging at least for these values of $J_1$.

The impact of row balance on the chaotic dynamics can be understood by noting that the resulting connectivity matrix, $\tilde{\mathbf{J}}$, now has a null-space, and the input mode, $\boldsymbol{\xi}$, lies within it ($\tilde{\mathbf{J}}\boldsymbol{\xi} = 0$). The result of row balance then is to ensure that the random connectivity matrix filters out any coherent activity fluctuations, $\bar{\phi}(t)$:

$$\tilde{\mathbf{J}}\boldsymbol{\phi} = \left(\mathbf{J} - \mathbf{J}\frac{1}{N}\boldsymbol{\xi}\cdot\boldsymbol{\xi}^T\right)\left(\bar{\phi}\boldsymbol{\xi} + \delta\boldsymbol{\phi}\right) = \mathbf{J}\delta\boldsymbol{\phi} \tag{12}$$

This prevents the coherent mode activity from driving feedback to the dynamics of the coherent current.

Strikingly, we find that row balance allows chaotic fluctuations to persist for larger values of $J_1$(Fig 2E), whereas without row balance the network reaches fixed points or limit cycles. Furthermore, the chaotic dynamics are more coherent with row balance than without (Fig 2F). As the structured connectivity is made stronger row balance appears to enable the dynamics to grow increasingly coherent even as chaotic fluctuations persist. We explore this phenomenon in the coming sections.

## Highly Coherent Chaos

One would expect that as the dynamics became more coherent, very quickly the residual fluctuations would become entirely drowned out, because of the saturation nonlinearity of $\phi$, driving the system out of the chaotic regime. Indeed, when sufficiently strong spatial coherence is induced by a symmetric connectivity, e.g., $J_1\frac{\boldsymbol{\xi}\boldsymbol{\xi}^T}{N}$, the system exhibits a coherent fixed point for sufficiently large $J_1$ [35, 16]. Surprisingly, we find that with row balance, increasing $J_1$ yields chaotic dynamics which are strikingly coherent and display switching-like macroscopic activity (Fig 3A).

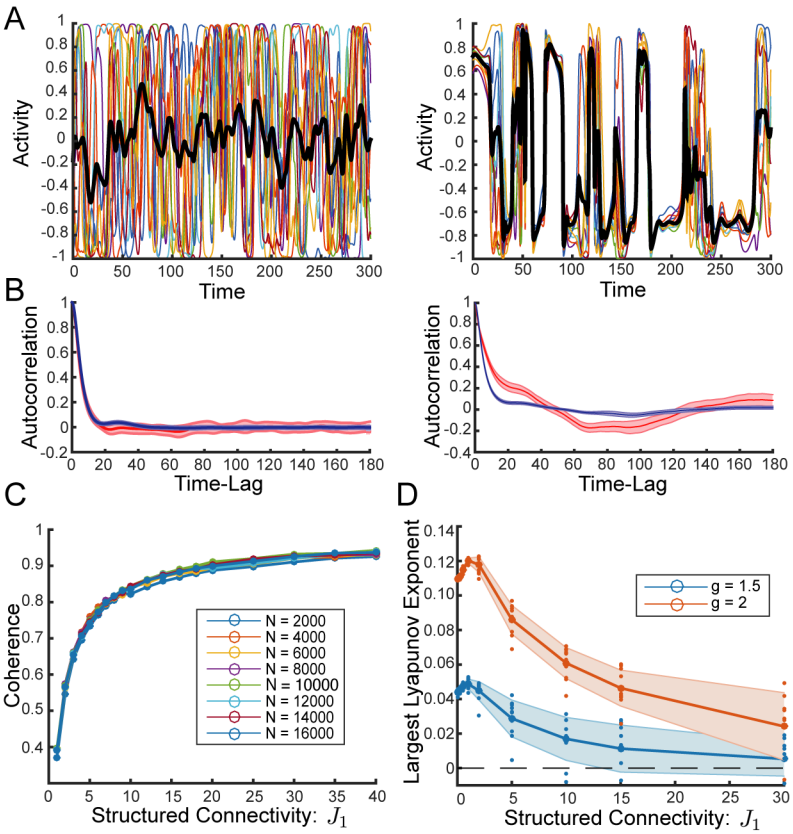


**Figure 3. Strong Structured Connectivity with Row Balance Generates High Coherence Even as Chaos Persists. (A)** Sample activity of 10 randomly chosen neurons, $\phi_j$, and coherent mode activity, $\bar{\phi}$, in black. Strong structured connectivity with row balance subtraction to the random component of connectivity yields chaotic activity that is highly coherent with switching-like behavior. **(B)** Normalized autocorrelation of coherent mode in red, and residual in blue. Shaded regions show standard deviation over 25 initial conditions of the same connectivity. Coherent mode dynamics are qualitatively different from those of the residuals. **(A)-(B)** $N = 4000$ Left: $J_1 = 0.8$. Right: $J_1 = 15.8$. **(C)** Coherence, $\chi$, as a function of $J_1$ for different network sizes exhibits universality. Coherence appears to approach 1 as $J_1$ is increased demonstrating that chaos persists even as fluctuations in the residuals shrink. Coherence is averaged over 30 realizations of the connectivity for each $N$, excluding the few fixed points and limit cycles that occur for larger $J_1$ (2 out of 30 or less for the largest values of $N$). **(D)** Largest Lyapunov exponent as a function of $J_1$. Thick line shows average over 10 realizations, small dots show values for individual realizations, and shaded region is standard deviation. All but a small fraction of realizations are chaotic, even in the region where $\chi > 0.9$. $g = 2$ in all panels unless noted otherwise.

In contrast to the mild-coherence regime, with strong structured connectivity the coherent mode dynamics are no longer passively driven by the fluctuations in the residual synaptic currents. This is evidenced by the normalized autocorrelation of the coherent mode, $\bar{q}(\tau)$, which is no longer close to the normalized residual autocorrelation, $q_\delta(\tau)$, but rather has qualitatively different dynamics including longer time-scales (Fig 3B).

We increase $J_1$ up to values of 100 and observe that chaos persists and coexists with a very high degree of spatial coherence. The coherence measure, $\chi$, increases with increasing $J_1$and reaches values higher than 0.96 even as fluctuations persist (Fig 3C and Fig S1). We calculate the largest Lyapunov exponent and verify that the dynamics are indeed chaotic for a vast majority of realizations even as the dynamics are highly coherent (Fig 3C).

### Transition to low-dimensional dynamics for strong structured connectivity

We observe that for fixed system size and for each particular realization of the random connectivity, there is a value of $J_1$ above which the network reaches either a fixed point or a limit cycle. This result has been previously observed and analyzed [8].

Each realization exhibits a phase transition in the parameter space of $J_1$vs $g$, and the critical curve $J_1^c(g)$ is monotonically increasing. The shape and location of this curve are realization dependent. (Fig 4A-B)

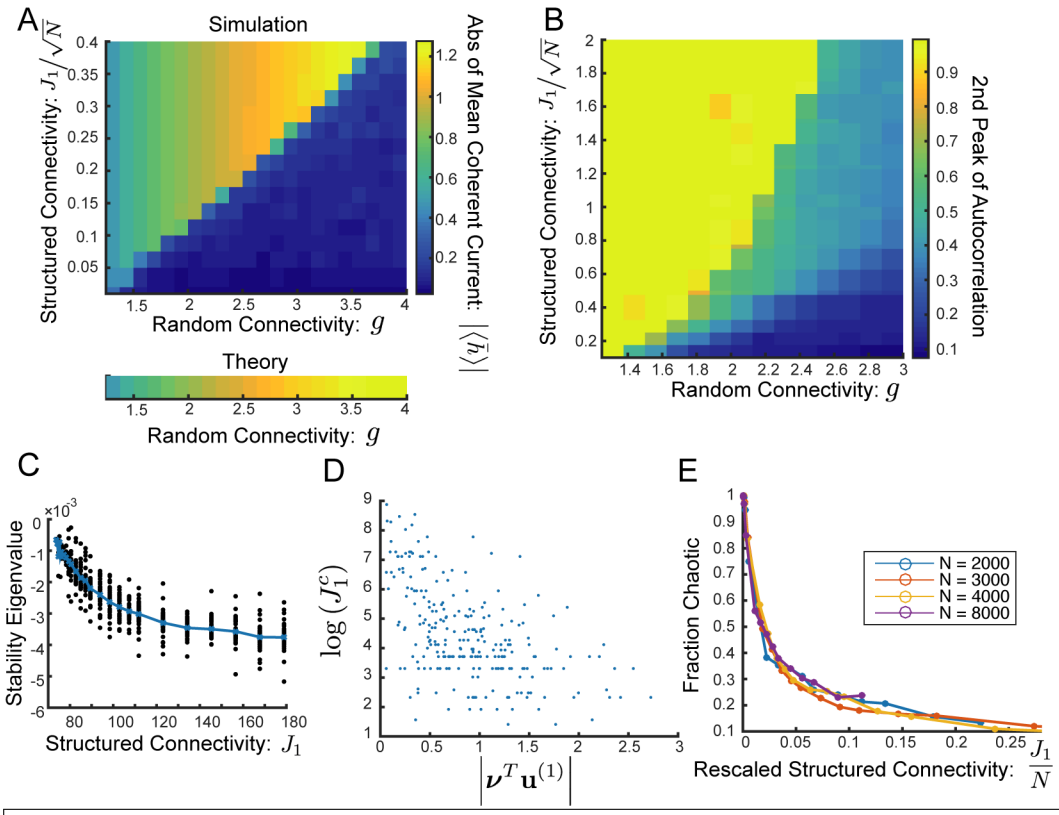


**Figure 4. Sufficiently Strong Structure Yields Transition Out of Chaos:** **(A)** Phase diagram for a single connectivity realization with real leading eigenvector. Colormaps the absolute value of the mean coherent current over a single trial, $|\langle\bar{h}\rangle|$ which is close to zero when the network is chaotic and non-zero when at a fixed point. The bar below shows the fixed point value predicted by theory, which is independent of $J_1$, as a function of $g$: $\phi'(h^*) = \frac{1}{g}$ **(B)** Phase diagram for a single connectivity realization with complex leading eigenvector. Colormap shows the second peak of the normalized autocorrelation of the coherent mode. This is 1 if the dynamics are perfectly oscillatory. $N = 4000$ for **(A)-(B)**. **(C)** Stability eigenvalue at fixed point, i.e. leading eigenvalue of the Jacobian, $-1 + \tilde{J}_{ij}\phi'(h_j)$, as a function of $J_1$ for a specific realization of the random connectivity. The fixed point exhibits marginal stability independent of $J_1$. **(D)** Scatterplot of the logarithm of transitional value of $J_1$ vs the absolute value of the projection of the output mode, $\boldsymbol{\nu}$, on the leading eigenvector, $\mathbf{u}^{(1)}$ for 300 connectivity realizations with $N = 8000$. $r^2 = 0.29$. **(E)** Fraction of realizations displaying chaotic activity as a function of the rescaled structured connectivity: $\frac{J_1}{N}$. With this scaling the curve appears to be independent of $N$.

As was previously shown[8], for a given realization of $\tilde{\mathbf{J}}$, for large enough $J_1$ the residual dynamics will be low dimensional and determined by the leading eigenvalue of $\tilde{\mathbf{J}}$. If this eigenvalue is real then the corresponding eigenvector is real and the resulting dynamics are a fixed point. If the leading eigenvalue is complex the resulting dynamics are

a limit cycle. We review these analytical results and report further numerical evidence in Methods and Supplementary. Here we briefly discuss the role of row balance in facilitating coherent, low-dimensional dynamics.

The crucial role of row balance is that it filters out the coherent component from the activity, as mentioned above ($\tilde{\mathbf{J}}\boldsymbol{\phi} = \mathbf{J}\delta\boldsymbol{\phi}$). When furthermore, the residual synaptic currents are small, $\delta h_i \ll 1$, we can approximate $\boldsymbol{\phi} \approx \phi\left(\bar{h}\right)\boldsymbol{\xi} + \phi'\left(\bar{h}\right)\delta\mathbf{h}$ and the dynamics of the residuals (Eqn 4) become linear:

$$\frac{\mathrm{d}\delta\mathbf{h}}{\mathrm{d}t} = -\delta\mathbf{h} + \phi'\left(\bar{h}\right)\hat{\mathbf{J}}\delta\mathbf{h} \tag{13}$$

We show in the Methods that $\hat{\mathbf{J}}$ has the same eigenvalues as $\tilde{\mathbf{J}}$. Note that had we ignored the constraint $\sum \xi_i \delta h_i = 0$ we might have expected the dynamics would be determined by the eigenvalues of $\mathbf{J}$, and these are not the same as those of $\hat{\mathbf{J}}$.

We write the eigenvectors of $\hat{\mathbf{J}}$ as $\mathbf{u}^{(i)}$ with $\hat{\mathbf{J}}\mathbf{u}^{(i)} = \lambda_i \mathbf{u}^{(i)}$, and the linear dynamics of the residuals (Eqn 13) can be decomposed along the eigenvectors by writing $\delta\mathbf{h} = \sum_i c_i \mathbf{u}^{(i)}$:

$$\frac{\mathrm{d}c_i}{\mathrm{d}t} = \left(-1 + \phi'\left(\bar{h}\right)\lambda_i\right)c_i \tag{14}$$

.

For a fixed point solution to exist the coherent mode $\bar{h}^*$ must be at the critical value for which

$$\phi'\left(\bar{h}^*\right) = \frac{1}{\lambda_1} \approx \frac{1}{g} \tag{15}$$

thus making the dynamics of $c_1$ marginal while all other components decay. Therefore the fixed point solution will have the residuals parallel to the leading eigenvector of $\hat{\mathbf{J}}$, i.e. $\delta\mathbf{h}^* = c_1\mathbf{u}^{(1)}$.

Substituting the critical value of $\bar{h}^*$ into the fixed point equation for the coherent mode ($\bar{h}^* = \frac{J_1}{\sqrt{N}}\boldsymbol{\nu}^T\delta\mathbf{h}^*$)fixes the scale factor, $c_1$,

$$c_1 = \frac{\bar{h}^* g}{J_1/\sqrt{N}\left(\boldsymbol{\nu}^T\mathbf{u}^{(1)}\right)} \tag{16}$$

We confirm numerically that this fixed point is reached above some critical curve $J_1^c(g)$, with $\left|\left\langle\bar{h}^*\right\rangle\right| \approx \phi'^{-1}\left(\frac{1}{g}\right)$ independent of the value of $J_1$(Fig 4A and Fig S2). Interestingly, this mechanism is reminiscent of self-organized criticality, namely the dynamics drive the system toward a marginal fixed point, without fine tuning of stability parameter. Indeed, we confirm numerically (Fig 4C), that independent of $J_1$ the fixed point has very small stability-

eigenvalue.

As we show in Methods, in the case of complex leading eigenvalue for $\tilde{\mathbf{J}}$(equivalently, $\hat{\mathbf{J}}$), the system converges to a limit cycle which also exhibits self-organized criticality. In that case the average slope of the transfer function $\phi'\left(\bar{h}\right)$ over each equals the critical value $1/g$ independent of $J_1$, and the frequency is given by the phase of the leading eigenvalue (Fig S3). The phase of the typical leading eigenvalue decreases with system size, and therefore the typical period of the limit cycle diverges as system size grows to infinity.

In conclusion, in both the fixed point and limit cycle solutions, the coherent component displays a self-organized criticality which enables the residuals to remain small.

Notice the crucial role of row balance, without which a fixed point with small residuals is not at all possible (since the coherent component of the activity is not cancelled out to yield homogeneous differential equations for the residuals and the coherent mode cannot play the role of dynamic gain, as in Eq. 13).

Note also the role of the binary structure of $\xi_j = \pm 1$ and the symmetry of the transfer function, which together yield $\phi\left(\xi_j x\right) = \xi_j \phi\left(x\right)$ and $\phi'\left(\xi_j x\right) = \phi'(x)$. We can loosen the constraint and use any smooth sigmoidal transfer function if we restrict the input mode to be uniform, $\xi_j = 1$ for all $j$.

We now consider the transition out of chaos. First, we expect that $J_1^c$ depends on the realizations of $\tilde{\mathbf{J}}$: Equation 16 suggests that $J_1^c$ scales as inverse of the overlap between the leading eigenvector, $\mathbf{u}^{(1)}$, and the output mode, $\boldsymbol{\nu}$ . Indeed, we show numerically that the critical value $J_1^c$ for fixed $g$ is negatively correlated with $\left|\boldsymbol{\nu}^T \mathbf{u}^{(1)}\right|$ (Fig 4D).

We next ask how $J_1^c$ scales with system size. Since, the typical value of $\left|\boldsymbol{\nu}^T \mathbf{u}^{(1)}\right|$is $O\left(1\right)$ we would naively expect that the typical transition might occur for $J_1^c \sim O\left(\sqrt{N}\right)$. However, we observe numerically that the fraction of realizations exhibiting chaotic dynamics for a given value of $J_1$ appears to scale as $\frac{J_1}{N}$ and not as $\frac{J_1}{\sqrt{N}}$ as expected (Fig 4D).

We conclude tentatively that in the limit of large system size chaos persists for all values of $J_1$. For finite $N$ chaos is lost for some $J_1^c \sim N^{\alpha}$with $\alpha \in [1/2, 1]$, and the particular $J_1^c$ is highly realization-dependent.

## Imprint of fixed point or limit cycle on the chaotic regime

From the previous analysis of the large $J_1$ regime in which fixed points or limit cycles arise ($J_1 \sim O\left(\sqrt{N}\right)$ at least), we can gain insight into the strongly coherent chaotic dynamics that exists for $J_1$ large but $O\left(1\right)$.

As mentioned above, for large values of $J_1$ the network dynamics exhibit coherent switching-like activity (Fig 5A top). Furthermore this activity appears to reflect a self-organized criticality as reflected in the speed of the dynamics. We define the speed as the norm of the vector of first time derivatives per neuron: $\sqrt{\frac{1}{N}\sum_i \left(\frac{\mathrm{d}h_i}{\mathrm{d}t}\right)^2}$. Measures such as the speed or its square have been used to find fixed points and slow dynamics in highly non-linear dynamics [32]. As shown in Fig 5A the chaotic trajectories frequently exhibits intervals with low speed. Additionally, the values of $\bar{h}$ come to deviate dramatically from Gaussian and instead become sharply bimodal (Fig 5B).

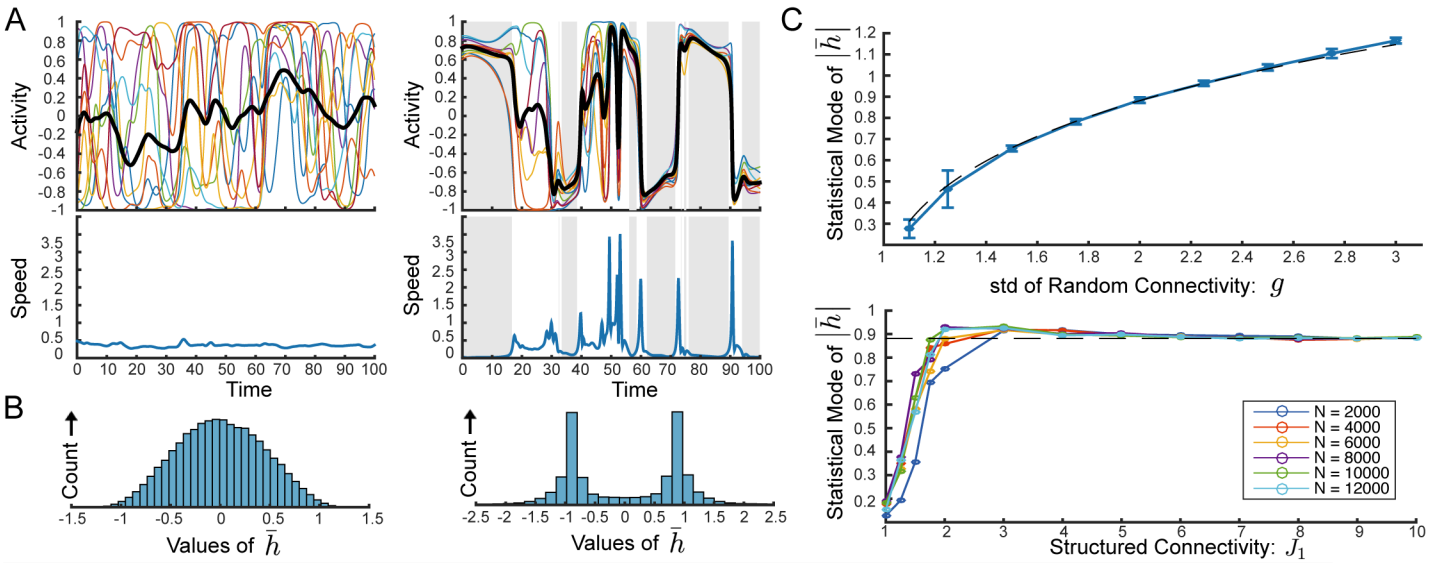


**Figure 5. Imprint of Self-Tuned Criticality on the Chaotic Regime.** **(A)** Top: Sample activity of 10 randomly chosen neurons and coherent mode activity, (same as Fig 3). Bottom: Speed of network during same epoch of activity, defined as the per-neuron norm of the rate-of-change vector, i.e. $\sqrt{\frac{1}{N}\sum_i \left(\frac{\mathrm{d}h_i}{\mathrm{d}t}\right)^2}$. For strong structured connectivity, bouts of high and low activity are associated with vanishing speed. **(B)** Histogram of values of the coherent mode current, $\bar{h}(t)$. For strong structured connectivity the histogram is bimodal. **(A)-(B)** Left: $J_1 = 0.8$. Right: $J_1 = 15.8$. **(C)** The statistical mode (most frequent value) of $|\bar{h}|$ as a function of $g$. Dashed line shows the theory prediction from the strong-structure limit, $\bar{h}^* = \sec^{-1}\left(\frac{1}{\sqrt{g}}\right)$. **(D)** Statistical mode of $|\bar{h}|$ as a function of $J_1$. A crossover occurs very rapidly and independently of $N$. Dashed line is $\bar{h}^*$. $N = 4000$ and $g = 2$ in all panels where not listed.

We can understand all these phenomena as an imprint of the low-dimensional dynamics of the large $J_1$ limit on the chaotic regime. We showed above that in both the fixed point and limit cycle solutions the coherent component displays a self-organized criticality which enables the residuals to remain small. This criticality is obtained in both cases at a coherent current with a (fixed or average) value of $\bar{h} = \phi'(1/g)$. We observe numerically that in the chaotic regime the coherent activity intermittently self-organizes near the same critical value yielding slow epochs at both low and high activity. In Fig 5A shaded regions show epochs during which the speed was slower than the slowest dynamics of a network without structured connectivity. We observe that epochs of both low and high activity are associated with very low speed, as well as very high coherence.

This switching between slow states yields a histogram of values of $\bar{h}(t)$ which is highly non-Gaussian and has a bimodal distribution of values with two distinct peaks at $\pm\phi'(1/g)$. We confirm numerically that the most common value of $|\bar{h}|$ as a function of $g$ fits the curve $\phi'^{-1}(1/g)$ very closely (Fig 5C). Evidently, epochs of high coherence emerge as the coherent mode activity comes near the critical point of $\phi'(\bar{h}) = \frac{1}{g}$ where the dynamics of the residuals are marginal and therefore slow.

Despite the fact that the transition out of chaos occurs only for $J_1 \sim O\left(\sqrt{N}\right)$ at least, we find that the bimodality of $\bar{h}$ with its peaks at critical values $\pm\phi'(1/g)$ arises already for values of $J_1$ that are $O(1)$ independent of $N$ (Fig 5C), which appears to reflect a distinct crossover from asynchronous to coherent chaos.

We also observe that in the case of a complex leading eigenvalue of $\tilde{\mathbf{J}}$, the chaotic regime exhibits signatures of oscillations, which are related to the realization-dependent phase of the complex eigenvalue, serving as a precursor of the full limit cycle for larger $J_1$. This is reflected in the presence of a large second peak in the autocorrelation function (Fig 6A). The height of this second peak grows gradually with $J_1$ throughout the chaotic regime, with a realization-dependent rate, until a pure limit cycle is reached and the second peak is near 1 (Fig 6B). Furthermore even within the chaotic regime, for most individual realizations the time of the second peak, which reflects the dominant frequency of the fluctuations, is well-predicted by the theoretical prediction for limit cycles: the phase of the leading eigenvalue (see Methods, Fig 6C).

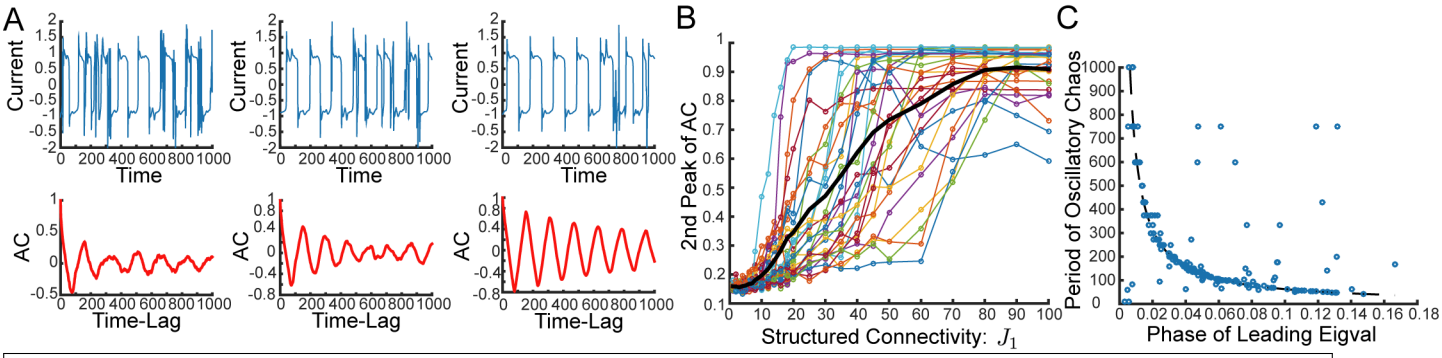


**Figure 6. Realization-Dependent Oscillatory Imprint on Chaotic Regime. (A)** Sample traces (top) and autocorrelation of coherent mode current (bottom) for a connectivity realization with complex eigenvalue for $J_1 = 25, 30, 35$. Dynamics exhibit pronounced oscillatory power and the autocorrelation exhibits a pronounced peak near the same frequency that will dominate the limit cycle for larger $J_1$. **(B)** Height of second peak of the autocorrelation of the coherent mode input as a function of $J_1$. Each colored line represents a single connectivity realization, averaged over 10 initial conditions. For many realizations, there is a significant second peak in the autocorrelation over a long range of values of $J_1$ well before a limit cycle is reached. We display the 30 realizations which had second peak larger than 0.8 for some $J_1$ within this range. Thick black line shows average over those realizations. **(C)** Observed period of oscillatory chaos vs phase of leading eigenvalue for 181 realizations from which we were able to measure an oscillatory period with chaotic fluctuations (confined to realizations and values of $J_1$ that yielded second peak of autocorrelation less than 0.8, mean second peak over all realizations: 0.5). Dotted line shows prediction from theory. The bulk of realizations are very well predicted although a notable fraction are not. The median error of prediction was 7.75 (average period: 231, std: 212). $N = 8000$ for all panels.

Likewise, in the case of a real leading eigenvalue, the chaotic dynamics exhibits an imprint of the fixed point. Each of the pair of fixed points (with $\pm\ \bar{h}^*$) break the $h \to -h$ symmetry of the underlying dynamics, depending on initial condition. Interestingly, we observe that before the transition to fixed point, the symmetry is broken already in the chaotic regime, with chaotic trajectories spending more time near one fixed point than the other depending on initial condition (Fig 7A). We measure the asymmetry in a single trial as the absolute value of the time-averaged coherent activity, $\left|\langle \bar{h} \rangle\right|$, and we find that asymmetry grows gradually with $J_1$ throughout the chaotic regime, and at different rates for different realizations (Fig 7B).

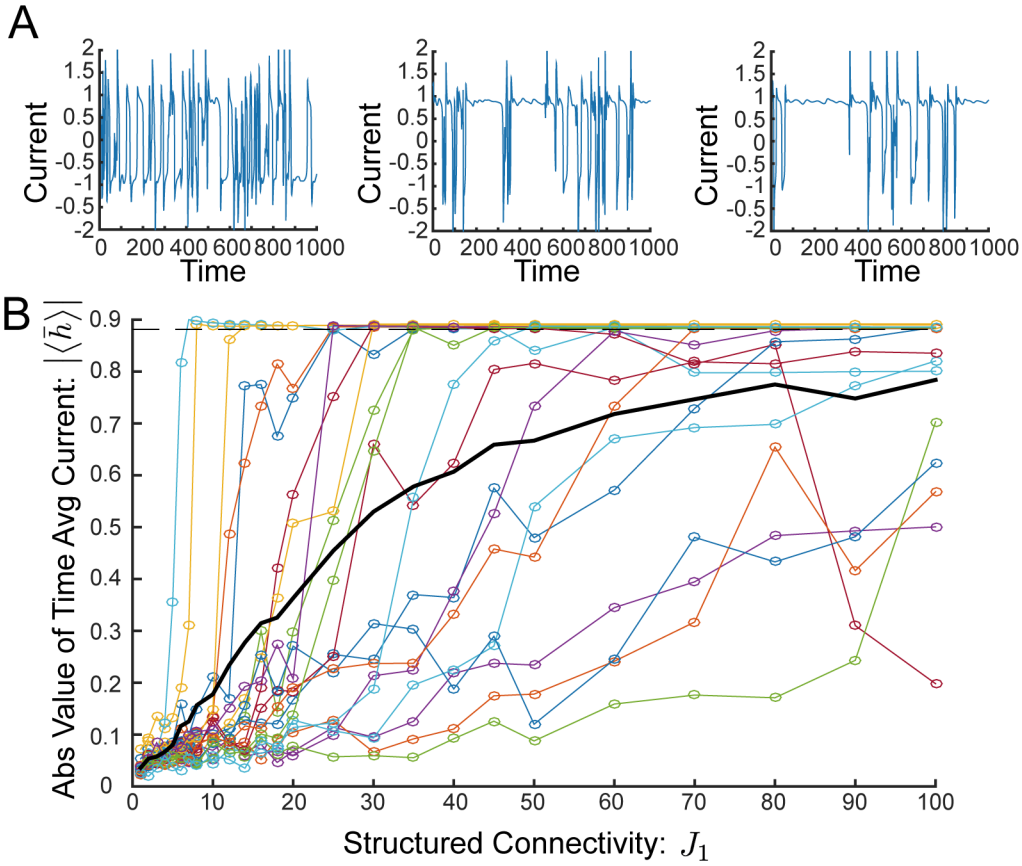


**Figure 7. Realization-Dependent Symmetry Breaking in Chaotic Regime.** **(A)** Sample traces of coherent mode input current from a connectivity realization with real eigenvalue for $J_1 = 40, 60, 80$ increasing from left to right. Dynamics exhibit pronounced asymmetry. **(B)** Absolute value of the time-average coherent mode input, $\left|\langle \bar{h} \rangle\right|$, as a function of $J_1$. Each colored line represents a single connectivity realization, averaged over 10 initial conditions. For many individual realizations, $\left|\langle \bar{h} \rangle\right|$ is significantly non-zero over a long range of values of $J_1$, while still not arriving at fixed point value (displayed by dashed line). We display the 20 realizations which had $\left|\langle \bar{h} \rangle\right| > 0.5$ for some $J_1$ within this range. Thick black line shows average over those realizations. $N = 8000$ for all panels.

## Multiple Modes of Coherence

We generalize our model in order to construct a network with multiple modes of coherent activity. In this extension we take the structural component, $\mathbf{M}$, to be a low-rank matrix comprised of the sum of outer products of pairs of

vectors which are all mutually orthogonal:

$$\mathbf{M} = J_0 \sum_{k=1}^{d} \frac{w_k}{\sqrt{N}} \boldsymbol{\xi}^{(k)} \boldsymbol{\nu}^{(k)^T} \tag{17}$$

where we have introduced a parameter $J_0$ that controls the overall strength of the structured connectivity, and a set of parameters $w_k$ satisfying $\sum_{k=1}^{d} w_k^2 = 1$ that determine the relative weight of the different modes.

We can extend our schematic representation and think of each row vector $\boldsymbol{\nu}^{(k)^T}$ as a separate output mode connected in a feed-forward-like manner to the input mode, $\boldsymbol{\xi}^{(k)}$, (Fig 8A) and then decompose the dynamics into the residual dynamics identical to the above (Eqn 4) and the dynamics of the coherent activity along each separate input mode:

$$\frac{\mathrm{d}\bar{h}^{(k)}}{\mathrm{d}t} = -\bar{h}^{(k)} + \frac{J_0 w_k}{\sqrt{N}} \boldsymbol{\nu}^{(k)^T} \boldsymbol{\phi} \tag{18}$$

where each the separate coherent activity is given by $\bar{h}^{(k)} \equiv \frac{1}{N} \sum_j \xi_j^{(k)} h_j$.

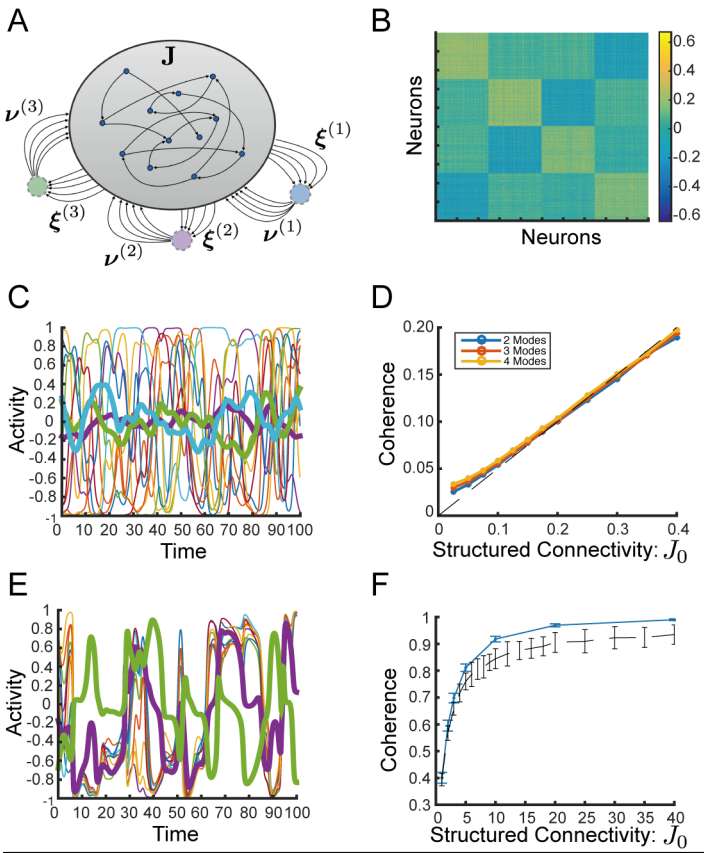


**Figure 8. Coherent Chaos Along Multiple Modes.** **(A)** Schematic of network with three coherent modes displaying effective output modes, $\boldsymbol{\nu}^{(k)}$, and input modes, $\boldsymbol{\xi}^{(k)}$, each of which are orthogonal to all others. **(B)** Matrix of Pearson correlation coefficients between firing rates, $\phi_i$, of pairs of neurons in a network with three coherent modes and $J_1 = 1$. **(C)** Sample activity trace displaying sample single neuron activities and in thicker lines, three coherent mode activities, $\bar{\phi}^{(k)}$. **(D)** Generalized coherence, $\chi^{(k)}$, as a function of $J_1$for 2, 3, 4 modes. Dashed line displays theory. **(E)** Sample activity traces display extreme coherence for two coherent modes. **(F)** Generalized coherence for two coherent modes as a function of $J_1$ extends to near complete coherence, while chaos persists. Compare network with one coherent mode with dashed line. Bar shows standard deviation over 100 realizations. $N = 2000$ for panels **(B)**, **(C)**, **(E)**. $N = 4096$ for panels **(D)** and **(F)**.

The analytical results found above for the regime of mild coherence can be directly extended to the case of multiple modes. In particular, in the limit where $J_0 \ll 1$, the separate coherent modes are independent of each other and driven passively by the residual fluctuations (Fig 8C ) such that

$$\bar{\Delta}^{(k)}(\tau) \approx \frac{J_0^2}{g^2} w_k^2 \Delta_\delta(\tau) \tag{19}$$

where $\bar{\Delta}^{(k)}(\tau) = \left\langle \bar{h}^{(k)}(t)\, \bar{h}^{(k)}(t+\tau) \right\rangle$ is the autocorrelation function of the $k$th coherent mode.

The resulting covariance matrix, $C_{ij} \equiv \langle \phi_i \phi_j \rangle$, has a low-rank structure which is given by the input modes (Fig 8B

). In particular, by Taylor expanding $\phi_i$ around $\delta h_i$:

$$C_{ij} \approx \left\langle \left( \phi\left(\delta h_i\right) + \phi'\left(\delta h_i\right) \sum_k \bar{h}^{(k)} \xi_i^{(k)} \right) \left( \phi\left(\delta h_j\right) + \phi'\left(\delta h_j\right) \sum_k \bar{h}^{(k)} \xi_j^{(k)} \right) \right\rangle \tag{20}$$

Since the residuals are on average uncorrelated and the distinct input modes are orthogonal, we find using Eqn 19 that to leading order:

$$\mathbf{C} \approx \left[\phi'\right]_{\mathbf{J}}^2 \Delta_\delta\left(0\right) \frac{J_0^2}{g^2} \sum_{k=1}^{d} w_k^2 \boldsymbol{\xi}^{(k)} \boldsymbol{\xi}^{(k)^T} \tag{21}$$

We generalize our measure of coherence to measure the $d$-dimensional coherence, or the fraction of total standard deviation which is captured by the $d$ coherent mode directions:

$$\chi^{(d)} \equiv \sqrt{\frac{\sum_{k=1}^{d} \left\langle \left(\bar{h}^{(k)}\right)^2 \right\rangle}{\frac{1}{N}\sum_i \left\langle h_i^2 \right\rangle}} \tag{22}$$

and we find that for $J_k \ll g$ and finite $d$

$$\chi^{(d)} \approx \frac{J_0}{g} \tag{23}$$

Numerically, this prediction holds well for up to $\frac{J_0}{g} = 0.2$ for at least up to $d = 4$ as we show in Fig 8D, and we expect it to hold for larger $d$ as well.

We note that in the regime of mild coherence, just as in the case of a single coherent mode, we can relax the restrictions on $\boldsymbol{\xi}^{(k)}$ and $\phi$: Our results hold for $\boldsymbol{\xi}^{(k)}$ any norm $\sqrt{N}$ vector orthogonal to $\boldsymbol{\nu}^{(j)}$ $\forall j$ and $\boldsymbol{\xi}^{(j)}$ $j \neq k$, and also for $\phi$ any sigmoidal function.

In addition, we can generalize row balance by subtracting the weighted row-average for each input mode such that every $\boldsymbol{\xi}^{(k)}$ will reside in the null space of the new connectivity matrix, $\tilde{\mathbf{J}}^{(d)}$:

$$\tilde{\mathbf{J}}^{(d)} \equiv \mathbf{J} - \mathbf{J} \cdot \frac{1}{N} \sum_{k=1}^{d} \boldsymbol{\xi}^{(k)} \cdot \boldsymbol{\xi}^{(k)^T} \tag{24}$$

For $d > 2$ this generalized row balance does not appear to preserve chaotic fluctuations and instead fixed points or limit cycles appear for $J_0 \sim O\left(1\right)$.

Intriguingly, for $d = 2$ we observe that with generalized row balance the chaotic regime persists as the structured connectivity is strengthened and the dynamics become increasingly coherent. The dynamics display switching-like activity in which at any time one of the two coherent modes appears to be near the critical value $h^c$ while the other mode is near zero (Fig 8E). It appears that the generalized coherence approaches 1 while chaos persists (Fig 8F)

such that we conjecture that just as in the case of $d = 1$, here too in the large $N$ limit $\chi^{(2)} \to 1$ as $J_0 \to \infty$.

## Discussion

Coherent fluctuations are prevalent in cortical activity ranging in spatial scale from shared variability in membrane potential and spiking in local circuits to global signals measured across the scalp via EEG or across voxels via fMRI [40, 27, 1, 14]. Constructing a model that intrinsically generates coherent fluctuations has been a challenge to theorists.

We have studied the generation of coherent chaotic dynamics in recurrent neural networks. Our model consists of rate-based neurons whose recurrent connections include a structured component in addition to random connections. The structured component is a low rank connectivity matrix consisting of outer products between orthogonal pairs of vectors which allow local fluctuations to be summed along an output mode, amplified and projected to an input mode resulting in coherent fluctuations. The orthogonality of input and output mode effectively embeds a purely feedforward structure within the recurrent connectivity, thus avoiding feedback of the coherent fluctuations along the input mode.

In the regime where the structured component is weak, the local synaptic currents are effectively uncoupled from the coherent mode activity and their dynamics are similar to that of a random network with no structured component at all. The local fluctuations are summed by the structured component of connectivity to drive the coherent mode, which follows those fluctuations in a passive manner. In this regime a perturbative dynamical mean-field theory following [30, 12] shows that the coherence grows linearly with the ratio of the strength of structured connectivity to the random connectivity. This analysis is easily extended to multiple modes of coherent activity yielding a finite-rank covariance pattern for the coherent fluctuations.

For strong structured component we observe highly coherent chaos in which the dynamics are dominated by a single mode of activity, which undergoes Up-Down-like switching. We show numerically that as the amplitude of the structured component is increased the dynamics become increasingly coherent. Above some critical strength of the structured component, the system converges on a either a fixed point or a limit cycle, depending on individual realization of the random connectivity. The critical amplitude grows with the system size, hence we propose that for all fixed values of structured component, as the network size diverges, coherent chaos persists regardless of the strength of structured component,

Our numerical work suggests that the typical critical strength of structure that yields a transition out of chaos most likely scales as $J_1 \sim O(N)$ (or at least as $J_1 \sim O\left(\sqrt{N}\right)$), but this requires more work to confirm. Surprisingly, the imprint of the fixed points and limit cycles on the chaotic dynamics is apparent already for moderate values of $J_1$. In particular, the Up and Down states we observe in the chaotic dynamics occur at the precise activity values that yield fixed points and up-down limit cycles for very large $J_1$. The crossover to dynamics of switching-like activity between these state occurs for $J_1 \sim O(1)$, independent of network size.

Importantly, in the regime of weak structured connectivity some of the assumptions of our model can be loosened. In this regime we need not require the input mode be binary but rather any general pair of orthogonal vectors can be used. This is in fact what we have done numerically in the section on multiple modes. Moreover we can loosen the restriction on orthogonality: a random pair of vectors can serve as input and output mode without qualitative impact on the dynamics presented here because the contribution of the realization-dependent overlap in this regime will be negligible relative to the typical contribution from the random component. The loosening of these constraints is encouraging as it may offer some promise that a biologically plausible synaptic learning rule could yield the necessary structured connectivity. Learning rules for yielding balanced excitation-inhibition dynamics may provide a foundation [39, 15, 13]. Additionally, prior studies of sequence generation, for example, have constructed learning rules that yield connectivity which is comprised of outer-products of random vectors [29, 33]. Deriving and verifying such a learning rule for generating coherent chaos, however, is beyond the scope of this work.

It should be stressed that the regime of strong structured connectivity and highly coherent chaos, on the other hand, requires the network be finely-tuned to a high degree. The orthogonality of the input and output modes is not enough in order to achieve highly coherent chaos because of interactions between the random and structured components of connectivity. We therefore constrain the random component to satisfy row balance by ensuring that the input mode of the structured connectivity be in the null-space of the random component of connectivity. We are less optimistic about the potential biological plausibility of this regime.

In addition to row balance, the high coherence regime depends on the choice of the single-neuron transfer function and input-mode vector. Our particular choice of hyperbolic tangent, which has been inherited from statistical physics, is an odd function: $\phi(\xi_i x) = \xi_i \phi(x)$ and $\phi'(\xi_i x) = \phi'(x)$ for $\xi_i = \pm 1$. The first equality acts in concert with the row balance to filter out the coherent-mode activity. The second equality guarantees that the coherent mode input acts as a dynamic-gain on the dynamics of the residuals in a uniform way. As mentioned in the main text, we can loosen the requirement of an odd transfer function at the cost of requiring a uniform input mode, $\xi_i = 1 \, \forall i$. The theory developed here predicts coherent fluctuations that switch between slow points where the slope of the transfer function is $1/g$, and we have verified this numerically (Fig S4).

In the case of a uniform input mode the model can be constructed as an excitation-inhibition network, for example with half the neurons defined as excitatory by setting $\nu_i = 1$ and the other half defined as inhibitory via $\nu_i = -1$ (or a larger inhibitory value to compensate for a smaller fraction of inhibitory neurons). From this perspective the coherent fluctuations can be understood within the framework of dynamic excitation-inhibition balance [38]. In this case the pair of balance equations are degenerate and constrain only the mean excitatory population rate to be nearly equal the inhibitory rate, but otherwise leave the overall mean rate unconstrained. Local residual fluctuations yield only small differences is mean population rates, thus leaving the balance satisfied, but these small differences drive significant coherent fluctuations because of the strong balanced connectivity . We note that excitation-inhibition networks in the literature have sometimes been constructed in this manner; with structured connectivity effectively consisting of a rank-one outer product of a pair of orthogonal vectors. As we have shown here, such choices have dramatic impact on the dynamics and the results should not be assumed to be generalizable.

In parallel to our study a pre-print has been published which explores a very similar model[10]. The authors observe a similar phenomenon numerically and write similar mean-field equations. Whereas we have focused on analytical solutions to these equations in the limit of both weak and strong structured connectivity, the authors develop an iterative approach to numerically solve the equations. They restrict their study to the case of a single orthogonal E-I structured component, and they appear to come to different conclusions about the realization-dependence and the role of row balance. As we have shown here row balance is critical for coherent chaos. Additionally we have explained the primary realization-dependence that appears in the limits of strong structured connectivity: either a fixed point or a limit cycle will emerge depending on the leading eigenvalue of the random connectivity matrix after row balance subtraction, and furthermore the transition to either fixed point or limit cycle is correlated with the extent of overlap between the leading eigenvector and the output mode.

As mentioned in the main text and introduction, a previous study also explored the case of a single orthogonal E-I structured component[8]. They derived the fixed point and limit cycle solutions which we reviewed here, but did not focus on the chaotic regime and they did not discuss the role of network size in the transition out of chaos. Our focus here was on the chaotic regime, both the emergence of coherence for small structured connectivity and the imprint of the non-chaotic regime on the chaotic dynamics for moderate structured connectivity.

A separate pre-print has claimed to observe coherent activity in excitation-inhibition networks of spiking neurons [37]. A study of the dynamics of spiking neurons is beyond the scope of our work, although we would conjecture that coherent activity would arise with orthogonal, rank-one E-I structure in that setting as well.

Previous work has shown how shared inputs from external drive can drive correlated fluctuations in excitation-inhibition networks [6, 25]. In our current work, in the context of rate neurons, we show that such correlated fluctuations can be generated internally by a recurrent network without external drive. In order to avoid either saturation or pure oscillations the coherent activity mode must not drive itself through a feedback loop. In order to achieve this it is necessary that the structured component embed an effectively-feedforward projection between a pair of orthogonal modes. In parallel, Darshan et al [5] have developed a theory for internally generated correlations in excitation-inhibition networks of binary units. The underlying principle is similar: the recurrent connectivity embeds a purely feedforward structure.

We note that the structured component of connectivity is non-normal. The dynamics of non-normal matrices have drawn a fair amount of interest with suggested functional impact on working memory [7, 9] and amplification [17]. In particular it has been shown that in networks with rank one E-I structure amplifies small differences between excitatory and inhibitory rates drive a large common response [17, 11], though the dynamics in those studies were linear. Non-normal matrices embed feedforward structure within recurrent connectivity, and the resulting dynamics even in a linear system are not fully determined by the eigenspectrum but depend on the structure of the corresponding eigenvectors[36]. Feedforward structure can be revealed by the Schur decomposition and the extent of feedforwardness can be measured as the fraction of total power (sum-of-squares) that is off the diagonal in the Schur decomposition. As pointed out in [2], a structured component such as in our model is purely feedforward and can be considered an extreme case of non-normality as it has only zero eigenvalues and therefore all its power is in the off-diagonal. The results here depend on this property and cannot be extended to connectivity with partially feedforward structure. Furthermore, the chaotic dynamics studied here are a distinctly non-linear effect and therefore the Schur decomposition alone gives little insight. We have instead focused our analytical work on the two regimes of weak and strong structured connectivity.

Rate model dynamics with a rank-one structured component have been studied in depth recently [24, 16]. Since these works focused on time-averaged activity and not fluctuations they did not observe coherent activity in the case of an outer product of a pair of orthogonal vectors as studied here. These works also differed in that the strength of the structured connectivity was scaled as $1/N$. This scaling is similar to our limit of weak structured connectivity, $J_1 \ll 1$, and guarantees that dynamic mean-field theory holds in the limit of large system size, but in that scaling coherent fluctuations will appear only as a finite-size correction.

It has been previously observed [22] and then proven [34] that adding an orthogonal outer-product to a random matrix generates realization-dependent outliers in the eigenspectrum, and furthermore that these outliers are be removed by row balance. It has been previously observed that performing such a subtraction has significant impact

on the resulting dynamics [8, 31]. Yet the relationship between the change in eigenspectrum and the dynamics has not been made clear beyond the basic observations regarding the stability of a fixed-point at zero. Here we suggest that the impact of row balance on the chaotic dynamics is not directly related to the eigenspectrum but that this adjustment should be thought of as effectively subtracting the coherent-mode activity from each individual neuron, thus decorrelating the residual currents. We show that row balance enables the emergence of slow residual dynamics with the coherent mode playing the role of dynamic gain, and that it is crucial for the emergence of highly coherent dynamics.

In conclusion we have presented a simple model which generates coherent chaos in which macroscopic fluctuations emerge through the interplay of random connectivity and a structured component that embeds a feedforward connection from an output mode to an orthogonal input mode.

# Methods

## Exact Decomposed Dynamics and Row Balance

We write the full dynamics without row balance:

$$\frac{\mathrm{d}\mathbf{h}}{\mathrm{d}t} = -\mathbf{h} + \mathbf{J}\boldsymbol{\phi} + \frac{J_1}{\sqrt{N}}\boldsymbol{\xi}\boldsymbol{\nu}^T\boldsymbol{\phi} \tag{25}$$

and we define

$$\bar{h} \equiv \frac{1}{N}\boldsymbol{\xi}^T\mathbf{h} \tag{26}$$

$$\delta\mathbf{h} \equiv \mathbf{h} - \boldsymbol{\xi}\bar{h} \tag{27}$$

Applying these definitions to the full dynamics (and noting that $\boldsymbol{\nu}^T\boldsymbol{\phi} = \boldsymbol{\nu}^T\delta\boldsymbol{\phi}$), the exact coherent mode dynamics are

$$\frac{\mathrm{d}\bar{h}}{\mathrm{d}t} = -\bar{h} + \frac{J_1}{\sqrt{N}}\boldsymbol{\nu}^T\delta\boldsymbol{\phi} + \frac{\boldsymbol{\xi}^T}{N}\mathbf{J}\boldsymbol{\phi} \tag{28}$$

and by subtracting these from the full dynamics of $\mathbf{h}$, the decomposed dynamics are:

$$\frac{\mathrm{d}\delta\mathbf{h}}{\mathrm{d}t} = -\delta\mathbf{h} + \mathbf{J}\boldsymbol{\phi} - \frac{\boldsymbol{\xi}\boldsymbol{\xi}^T}{N}\mathbf{J}\boldsymbol{\phi} = -\delta\mathbf{h} + \hat{\mathbf{J}}\boldsymbol{\phi} \tag{29}$$

where $\hat{\mathbf{J}} \equiv \left(\mathbf{I} - \frac{\boldsymbol{\xi}\boldsymbol{\xi}^T}{N}\right)\mathbf{J}$ as introduced in the main text.

We observe that the constraint $\boldsymbol{\xi}^T\delta\mathbf{h} = 0$ must be satisfied automatically by the residual dynamics (Eqn 29),

and this can be confirmed by verifying that

$$\frac{\mathrm{d}\left(\boldsymbol{\xi}^T \delta \mathbf{h}\right)}{\mathrm{d}t} = -\left(\boldsymbol{\xi}^T \delta \mathbf{h}\right) \tag{30}$$

In the regime where $J_1 \ll 1$ the $\phi_j$ are nearly uncorrelated and therefore $\frac{\boldsymbol{\xi}^T}{N}\mathbf{J}\boldsymbol{\phi} \sim O\left(\frac{1}{\sqrt{N}}\right)$ and can be ignored.

In the regime with strong structured connectivity we must consider this term in Eqn 28. To that end we write $\boldsymbol{\phi} = \bar{\phi}\boldsymbol{\xi} + \delta\boldsymbol{\phi}$ and also write the transformation of the input mode via the random matrix as

$$\mathbf{J}\boldsymbol{\xi} = a_{\parallel}\boldsymbol{\xi} + \boldsymbol{\xi}^{\perp} \tag{31}$$

where $a_{\parallel}$ is a realization-dependent scalar and $\boldsymbol{\xi}^{\perp}$ is a realization-dependent vector orthogonal to $\boldsymbol{\xi}$.

That yields coherent mode dynamics

$$\frac{\mathrm{d}\bar{h}}{\mathrm{d}t} = -\bar{h} + \frac{J_1}{\sqrt{N}}\boldsymbol{\nu}^T \delta\boldsymbol{\phi} + a_{\parallel}\bar{\phi} + \frac{\boldsymbol{\xi}^T}{N}\mathbf{J}\delta\boldsymbol{\phi} \tag{32}$$

and residual dynamics

$$\frac{\mathrm{d}\delta\mathbf{h}}{\mathrm{d}t} = -\delta\mathbf{h} + \hat{\mathbf{J}}\delta\boldsymbol{\phi} + \bar{\phi}\boldsymbol{\xi}^{\perp} \tag{33}$$

As $J_1$ increases and the fluctuations in the coherent activity, $\bar{\phi}(t)$, drive feedback in two ways. First of all, $\mathbf{J}$ maps the coherent activity back along the input mode driving direct feedback to the coherent current $\bar{h}$ via the term $a_{\parallel}\bar{\phi}$.

Secondly, $\mathbf{J}$ maps the coherent activity in a realization-dependent direction, $\boldsymbol{\xi}^T$, orthogonal to the input mode. This drives the residual activity fluctuations $\delta\mathbf{h}$ via the term $\bar{\phi}\boldsymbol{\xi}^{\perp}$, and this biasing of the residual fluctuations may in turn generate feedback to the coherent current through the output mode via $\boldsymbol{\nu}^T\delta\boldsymbol{\phi}$.

Both of these feedback terms are realization dependent, and both of them are canceled via the row balance subtraction

$$\tilde{\mathbf{J}} \equiv \mathbf{J} - \mathbf{J}\frac{\boldsymbol{\xi}\boldsymbol{\xi}^T}{N} \tag{34}$$

which yields coherent mode dynamics

$$\frac{\mathrm{d}\bar{h}}{\mathrm{d}t} = -\bar{h} + \frac{J_1}{\sqrt{N}}\boldsymbol{\nu}^T\delta\boldsymbol{\phi} + \frac{\boldsymbol{\xi}^T}{N}\mathbf{J}\delta\boldsymbol{\phi} \tag{35}$$

and residual dynamics

$$\frac{\mathrm{d}\delta\mathbf{h}}{\mathrm{d}t} = -\delta\mathbf{h} + \hat{\mathbf{J}}\delta\boldsymbol{\phi} \tag{36}$$

And in this case the residual dynamics are again uncorrelated so that $\frac{\boldsymbol{\xi}^T}{N}\mathbf{J}\delta\boldsymbol{\phi} \sim O\left(\frac{1}{\sqrt{N}}\right)$ and can again be ignored.

Note that $\bar{\phi}$ no longer drives feedback to either the residual or the coherent dynamics. Nevertheless the dynamics are still coupled in both directions as $\delta\boldsymbol{\phi}$ depends on $\bar{h}$.

## Perturbative Dynamic Mean-Field Theory

We derive the dynamic mean-field equations in the limit of small $J_1$ using a perturbative approach. We assume the residual currents $\delta h_i$ fluctuate as independent Gaussian processes, and then following previous results [30, 12], the autocorrelation of the residuals, $\Delta_\delta(\tau) = \langle \delta h_i(t)\, \delta h_i(t+\tau)\rangle$ is given by the self-consistency equation:

$$\left(1 - \frac{\partial^2}{\partial\tau^2}\right)\Delta_\delta(\tau) = g^2 C(\tau) \tag{37}$$

where $C(\tau)$ is the autocorrelation of the activity: $C(\tau) \equiv \langle \phi_i(t)\, \phi_i(t+\tau)\rangle$.

For $J_1 \ll g$ we assume that $\left|\bar{h}\right| \ll 1$, so that we have to leading order $\phi_i = \phi\left(\delta h_i + \xi_i\bar{h}\right) \approx \phi(\delta h_i)$. Thus to leading order the autocorrelation of the activity, $C(\tau)$, is given by integrating over two correlated Gaussians with autocorrelation $\Delta_\delta(\tau)$. Following previous work directly this can be written as

$$C(\tau) \approx \int_{-\infty}^{\infty} Dz \left(\int_{-\infty}^{\infty} Dx\, \phi\left(\sqrt{\Delta_\delta(0) - \Delta_\delta(\tau)}x + \sqrt{\Delta_\delta(\tau)}z\right)\right)^2 \tag{38}$$

Note that it is possible to compute the sub-leading correction term as well, but for our purposes this is unnecessary. We suffice it to observe that to leading order, the self-consistency equation for $\Delta_\delta(\tau)$ (Eqn 37) reduces to the identical equation for that of a random network without structured component[30]. Thus $\Delta_\delta(\tau) \approx \Delta_0(\tau)$, where $\Delta_0(\tau)$ is the autocorrelation when $J_1 = 0$.

Therefore the $\delta h_j$ are nearly independent and we can treat the sum $\frac{1}{\sqrt{N}}\sum_j \nu_j\phi_j$, which is the drive to $\bar{h}$ (Eqn 5), as a Gaussian process which itself has autocorrelation approximately given by $C(\tau)$. This yields an equation for

the coherent mode autocorrelation, $\bar{\Delta}(\tau) \equiv \left\langle \bar{h}(t)\, \bar{h}(t+\tau) \right\rangle$:

$$\left(1 - \frac{\partial^2}{\partial \tau^2}\right) \bar{\Delta}(\tau) \approx J_1^2 C(\tau) \tag{39}$$

Note that because $\phi_i \approx \phi(\delta h_i)$, the dynamics of $\bar{h}$ are to leading order driven passively by the fluctuations in $\delta h_i$. This is reflected in Eqn 39 which is not a self-consistency equation for $\bar{\Delta}(\tau)$ because $C(\tau)$ has already been determined by Eqn 37. Furthermore, the two equations are identical except for the coefficients so that we conclude that to leading order the resulting coherent autocorrelation is

$$\bar{\Delta}(\tau) \approx \frac{J_1^2}{g^2} \Delta_0(\tau) \tag{40}$$

Thus for $J_1 \ll g$ fluctuations in the coherent input are driven passively by the random source which is generated self-consistently by the residual fluctuations, and the resulting autocorrelation of the coherent mode is simply a scaled version of the autocorrelation of the residuals.

## Analysis of Fixed Points and Limit Cycles

In the limit of large $J_1$ we assume $\delta h_i \ll 1$, and approximate $\phi_j \approx \phi\left(\xi_j \bar{h}\right) + \phi'\left(\bar{h}\right) \delta h_j$, where we have made use of the symmetry of the transfer function and the binary restriction on $\xi_j$. Note that this linearization clearly holds without symmetric transfer function for the case of uniform $\xi_j = 1$ as well.

Following the exact decomposition above (Eqns 29 and 28)this yields dynamical equations:

$$\frac{\mathrm{d}\delta \mathbf{h}}{\mathrm{d}t} = -\delta \mathbf{h} + \phi'\left(\bar{h}\right) \hat{\mathbf{J}} \delta \mathbf{h} \tag{41}$$

$$\frac{\mathrm{d}\bar{h}}{\mathrm{d}t} = -\bar{h} + \frac{J_1}{\sqrt{N}} \phi'\left(\bar{h}\right) \boldsymbol{\nu}^T \delta \mathbf{h} + \phi'\left(\bar{h}\right) \frac{\boldsymbol{\xi}^T}{N} \mathbf{J} \delta \mathbf{h} \tag{42}$$

Note that the leading term of the linearization, $\phi\left(\xi_i \bar{h}\right) = \xi_i \phi\left(\bar{h}\right)$ has fallen from all terms, so that in this regime the coupling between residuals and coherent mode has been greatly simplified: The residuals serve as the input while the coherent mode acts as a dynamic gain This reflects the important role of the orthogonality of $\boldsymbol{\nu}$ and $\boldsymbol{\xi}$ on the one hand, and the row balance subtraction we made to the random connectivity, both of which ensure that the coherent mode does not drive a feedback loop.

In this regime $\bar{h}$ acts as a dynamic gain on the local synaptic currents through $\phi'\left(\bar{h}\right)$. Given $\bar{h}$ the equation for the

residual currents is linear and therefore their dynamics can be decomposed in the eigenbasis of the matrix

$$\hat{\mathbf{J}} \equiv \mathbf{P}_\xi \mathbf{J} \tag{43}$$

where $\mathbf{P}_\xi = \mathbf{I} - \frac{\boldsymbol{\xi}\boldsymbol{\xi}^T}{N}$ is the projection matrix onto the the subspace orthogonal to $\boldsymbol{\xi}$.

We claim that $\hat{\mathbf{J}} = \mathbf{P}_\xi \mathbf{J}$ and $\tilde{\mathbf{J}} = \mathbf{J}\mathbf{P}_\xi$ have the same eigenvalues. If $\lambda$ is an eigenvalue $\mathbf{J}$ such that the associated eigenvector $\mathbf{u}$ is orthogonal to $\boldsymbol{\xi}$, then clearly $\mathbf{u}$ is also an eigenvector of both $\hat{\mathbf{J}}$ and $\tilde{\mathbf{J}}$ with the same eigenvalue $\lambda$. Otherwise $\lambda$ is an eigenvalue of both $\hat{\mathbf{J}}$ and $\tilde{\mathbf{J}}$ if and only if $(\mathbf{J} - \lambda\mathbf{I})^{-1}\boldsymbol{\xi} = \mathbf{u}$ is orthogonal to $\boldsymbol{\xi}$. In this case it can be readily verified that $\mathbf{u}$ is an eigenvector of $\hat{\mathbf{J}}$, and $\mathbf{J}\mathbf{u} = \lambda\mathbf{u} + \boldsymbol{\xi}$ is an eigenvector of $\tilde{\mathbf{J}}$. Thus we note that the eigenvectors of $\hat{\mathbf{J}}$are orthogonal to $\boldsymbol{\xi}$ (except potentially for one eigenvector with zero eigenvalue).

We write the eigenvectors as $\mathbf{u}^{(i)}$ with $\hat{\mathbf{J}} \cdot \mathbf{u}^{(i)} = \lambda_i \mathbf{u}^{(i)}$. Writing the vector of residual current as $\delta\mathbf{h} = \sum_i c_i \mathbf{u}^{(i)}$ yields dynamics

$$\frac{\mathrm{d}c_i}{\mathrm{d}t} = \left(-1 + \phi'\left(\bar{h}\right)\lambda_i\right) c_i \tag{44}$$

The only (marginally) stable, non-zero fixed point is achieved with $c_1 \neq 0$ and $c_i = 0$ for all $i > 1$. And the fixed-point equation is

$$c_1^* \left(1 - \phi'\left(\bar{h}\right)\lambda_1\right) = 0 \tag{45}$$

This fixed point only exists if $\lambda_1$ is real, and yields a fixed-point requirement for $\bar{h}^*$:

$$\bar{h}^* = \phi'^{-1}\left(\frac{1}{\lambda_1}\right) \approx \phi'^{-1}\left(\frac{1}{g}\right) \tag{46}$$

In order to close the loop we turn to the fixed point equation for the coherent dynamics. Ignoring the term $\phi'\left(\bar{h}\right)\frac{\boldsymbol{\xi}^T}{N}\mathbf{J}\delta\mathbf{h}$, which yields an $O\left(\frac{1}{\sqrt{N}}\right)$ correction we find:

$$\bar{h}^* = \frac{J_1}{\sqrt{N}}\phi'\left(\bar{h}\right)\boldsymbol{\nu}^T\delta\mathbf{h}^* \tag{47}$$

which in turn, using $\delta\mathbf{h}^* = c_1\mathbf{u}^{(1)}$, yields a solution to leading order for $c_1$: $c_1^* = \frac{\bar{h}^*\lambda_1}{J_1/\sqrt{N}\left(\boldsymbol{\nu}^T\mathbf{u}^{(1)}\right)}$, as reported in [8].

If $\lambda_1$ is complex there is no fixed-point but rather a limit-cycle solution to the dynamics of the complex-valued $c_1$ exists, assuming $c_i = 0$ for all $i > 1$. Assuming $\bar{h}\left(t\right)$ is periodic with period $T$, we can separate variables and

integrate Eqn 44 in order to find $c_1(t)$ is given by

$$c_1(t) = c_1(0)\exp\left(-t + \lambda_1 \Phi(t)\right) \tag{48}$$

for $t \leq T$, where $\Phi(t) = \int_0^t \mathrm{d}s\, \phi'\left(\bar{h}(s)\right)$. A limit-cycle in phase with $\bar{h}(t)$ means $c_1(T) = c_1(0)$ and this requires that both $\mathrm{Re}[\lambda_1]\,\Phi(T) = T$ and also $\mathrm{Im}[\lambda_1]\,\Phi(T) = 2\pi$. From the first requirement we find that the average value of $\phi'$ over a period must be the critical value: $\langle \phi' \rangle = \frac{\Phi(T)}{T} = \frac{1}{\mathrm{Re}\lambda_1} \approx \frac{1}{g}$. And combining the second requirement yields an expression for the period (as reported in [8]):

$$T = 2\pi \frac{\mathrm{Re}\lambda_1}{\mathrm{Im}\lambda_1} \tag{49}$$

Simulations confirm that a projection of the full synaptic current dynamics into the coherent mode and the leading eigenvector plane (consisting of real and imaginary parts of $\mathbf{u}^{(1)}$) accounts for well over 0.99 of the total variance. Even restricting ourselves to the variance of the residuals, $\delta h_i$, we find that 0.98 of the variance is restricted to the leading eigenvector plane (Fig S3).

For $N = 4000$ we simulate 219 realizations of random connectivity with complex leading eigenvalue and find that for sufficiently large $J_1$ all but one of these realizations yield highly oscillatory dynamics with period predicted nearly perfectly by theory (Fig S3).

We note that in the limit of large $N$ we expect that the typical size of the imaginary component of the leading eigenvalue, $\lambda_1$, shrinks such that the typical period grows. These longer period oscillations are characterized by square-wave-like shape in which the dynamics of the coherent component slows around the critical value $\bar{h}^c = \phi^{-1}\left(\frac{1}{\mathrm{Re}\lambda_1}\right)$, which is identical to the fixed-point value of $\bar{h}$ when $\lambda_1$ is real. (Fig S3)

## Lyapunov Exponent, Limit Cycles, and Fixed Points

In order to calculate the largest Lyapunov exponent, we begin with a point $\mathbf{h}_0$ along the trajectory of the dynamics and we solve concurrently for the dynamics of the trajectory, $\mathbf{h}(t)$ with $\mathbf{h}(0) = \mathbf{h}_0$, and for a randomly chosen perturbation, $\boldsymbol{\eta}(t)$. The trajectory $\mathbf{h}(t)$ yields the time-dependent Jacobian matrix for each point along the trajectory:

$$\mathcal{J}_{ij}(t) = -1 + J_{ij}\phi'\left(h_j(t)\right) \tag{50}$$

We choose a random unit-norm vector $\boldsymbol{\eta}(0) = \boldsymbol{\eta}_0$ and iterate the linearized dynamics of the perturbation:

$$\frac{\mathrm{d}\boldsymbol{\eta}}{\mathrm{d}t} = \boldsymbol{\mathcal{J}}\boldsymbol{\eta} \tag{51}$$

The largest Lyapunov exponent is given by

$$\lim_{t\to\infty} \frac{1}{t} \log \|\boldsymbol{\eta}(t)\| \tag{52}$$

In practice we iterate 51 until $t = 5000$, that is, 5000 times the intrinsic time-scale of the dynamics, and we renormalize $\boldsymbol{\eta}(t)$ at intervals of $t = 100n$ for $n = \{1, 2, ..., 50\}$.

We classify fixed points numerically by a threshold on the fluctuations of the coherent input: $\mathrm{std}\left(\bar{h}(t)\right) \leq 5\mathrm{x}10^{-4}$.

We classify limit cycles by a threshold on the second peak of the normalized coherent autocorrelation: $q_{peak} \geq 0.9$.

We confirm that all of the trials with negative Lyapunov exponent were categorized as either fixed points or limit cycles. A small fraction of trials classified as limit cycles had positive Lyapunov exponents but with the largest one 0.0043.

# Acknowledgements

We thank Rainer Engelken for advice on numerically calculating Lyapunov exponents, and Yu Hu for very helpful comments on the manuscript. We thank the reviewers for thorough questions that helped clarify the manuscript. This work was funded by the Gatsby Charitable Foundation and the NIH.

# References

[1] Peter Achermann, Thomas Rusterholz, Roland Dürr, Thomas König, and Leila Tarokh. Global field synchronization reveals rapid eye movement sleep as most synchronized brain state in the human EEG. *Royal Society Open Science*, 3(10):160201, 2016.

[2] Yashar Ahmadian, Francesco Fumarola, and Kenneth D. Miller. Properties of networks with partially structured and partially random connectivity. *Physical Review E - Statistical, Nonlinear, and Soft Matter Physics*, 91(1):1–36, 2015.

[3] Anne K. Churchland, R. Kiani, R. Chaudhuri, Xiao Jing Wang, Alexandre Pouget, and M. N. Shadlen. Variance as a Signature of Neural Computations during Decision Making. *Neuron*, 69(4):818–831, 2011.

[4] Marlene R. Cohen and John H.R. Maunsell. Attention improves performance primarily by reducing interneuronal correlations. *Nature Neuroscience*, 12(12):1594–1600, 2009.

[5] Ran Darshan, Carl van Vreeswijk, and David Hansel. Strength of correlations in strongly recurrent neural networks. *Physical Review X*, 2018.

[6] Ran Darshan, William E. Wood, Susan Peters, Arthur Leblois, and David Hansel. A canonical neural mechanism for behavioral variability. *Nature Communications*, 8(May):15415, 2017.

[7] Surya Ganguli, Dongsung Huh, and Haim Sompolinsky. Memory traces in dynamical systems. *Proceedings of the ...*, 105(48):18970–18975, 2008.

[8] Luis Carlos García Del Molino, Khashayar Pakdaman, Jonathan Touboul, and Gilles Wainrib. Synchronization in random balanced networks. *Physical Review E - Statistical, Nonlinear, and Soft Matter Physics*, 88(4):1–5, 2013.

[9] Mark S Goldman. Memory without Feedback in a Neural Network. *Neuron*, 61(4):621–634, 2009.

[10] Takashi Hayakawa and Tomoki Fukai. Spontaneous and stimulus-induced coherent states of dynamically balanced neuronal networks. *arXiv*, (1):1–36, 2018.

[11] Guillaume Hennequin, Tim P. Vogels, and Wulfram Gerstner. Non-normal amplification in random balanced neuronal networks. *Physical Review E - Statistical, Nonlinear, and Soft Matter Physics*, 86(1):1–12, 2012.

[12] Jonathan Kadmon and Haim Sompolinsky. Transition to chaos in random neuronal networks. *Physical Review X*, 5(4):1–28, 2015.

[13] Itamar D Landau, Robert Egger, Vincent J Dercksen, Marcel Oberlaender, and Haim Sompolinsky. The Impact of Structural Heterogeneity on Excitation-Inhibition Balance in Cortical Networks. *Neuron*, 92:http://dx.doi.org/10.1016/j.neuron.2016.10.027, 2016.

[14] Thomas T. Liu, Alican Nalci, and Maryam Falahpour. The global signal in fMRI: Nuisance or Information? *NeuroImage*, 150(February):213–229, 2017.

[15] Yotam Luz and Maoz Shamir. Balancing feed-forward excitation and inhibition via Hebbian inhibitory synaptic plasticity. *PLoS computational biology*, 8(1):e1002334, jan 2012.

[16] Francesca Mastrogiuseppe and Srdjan Ostojic. Linking connectivity, dynamics and computations in recurrent neural networks. *Neuron*, 99(3):609–623.e29, 2018.

[17] Brendan K Murphy and Kenneth D Miller. Balanced Amplification: A New Mechanism of Selective Amplification of Neural Activity Patterns. *Neuron*, 61(4):635–648, 2009.

[18] Kevin Murphy and Michael D. Fox. Towards a consensus regarding global signal regression for resting state functional connectivity MRI. *NeuroImage*, 154:169–173, 2017.

[19] P L Nunez, R B Silberstein, M R Carpentar, R Srinivisan andR.S. Wijesinghe, D M Tucker, P J Cadusch, and X Wu. EEG coherency II: Experimental comparison of multiple measures. *Electroenceaphlogr Clin Neurophysiol*, 110:469, 1999.

[20] M. Okun, P. Yger, S. L. Marguet, F. Gerard-Mercier, A. Benucci, S. Katzner, L. Busse, M. Carandini, and K. D. Harris. Population Rate Dynamics and Multineuron Firing Patterns in Sensory Cortex. *Journal of Neuroscience*, 32(48):17108–17119, 2012.

[21] Michael Okun, Nicholas a. Steinmetz, Lee Cossell, M. Florencia Iacaruso, Ho Ko, Péter Barthó, Tirin Moore, Sonja B. Hofer, Thomas D Mrsic-Flogel, Matteo Carandini, and Kenneth D Harris. Diverse coupling of neurons to populations in sensory cortex. *Nature*, 2015.

[22] Kanaka Rajan and L F Abbott. Eigenvalue Spectra of Random Matrices for Neural Networks. *Physical Review Letters*, 97(18):188104, nov 2006.

[23] Alfonso Renart, Jaime De Rocha, Peter Bartho, Liad Hollender, Néstor Parga, Alex Reyes, and Kenneth D Harris. The Asynchronous State in Cortical Circuits. *Science (New York, N.Y.)*, 327(January):587–590, 2010.

[24] Alexander Rivkind and Omri Barak. Local Dynamics in Trained Recurrent Neural Networks. *Physical Review Letters*, 118(25):1–5, 2017.

[25] Robert Rosenbaum, Matthew A Smith, Adam Kohn, Jonathan E Rubin, and Brent Doiron. The spatial structure of correlated neuronal variability. *Nature Neuroscience*, 20(October):1–35, 2016.

[26] M. L. Scholvinck, A. Maier, F. Q. Ye, J. H. Duyn, and D. A. Leopold. Neural basis of global resting-state fMRI activity. *Proceedings of the National Academy of Sciences*, 107(22):10238–10243, 2010.

[27] Matthew a Smith and Adam Kohn. Spatial and temporal scales of neuronal correlation in primary visual cortex. *The Journal of neuroscience : the official journal of the Society for Neuroscience*, 28(48):12591–603, nov 2008.

[28] W R Softky and C Koch. The highly irregular firing of cortical cells is inconsistent with temporal integration of random EPSPs. *The Journal of neuroscience : the official journal of the Society for Neuroscience*, 13(1):334–50, jan 1993.

[29] H. Sompolinsky and I. Kanter. Temporal association in asymmetric neural networks. *Physical Review Letters*, 57(22):2861–2864, 1986.

[30] Haim Sompolinsky, A. Crisanti, and H. J. Sommers. Chaos in random neural networks. *Physical Review ...*, 61(3):259–262, 1988.

[31] Merav Stern and L F Abbott. Dynamics of rate-model networks with seperate excitatory and inhibitory populations. *The annual meeting of the Society for Neuroscience*, 2016.

[32] David Sussillo and Omri Barak. Opening the black box: low-dimensional dynamics in high-dimensional recurrent neural networks. *Neural computation*, 25(3):626–49, mar 2013.

[33] David W Tank and J J Hopfield. Neural computation by concentrating information in time. *Proceedings of the National Academy of Sciences*, 84(April):1896–1900, 1987.

[34] Terence Tao. Outliers in the spectrum of iid matrices with bounded rank perturbations. *Probability Theory and Related Fields*, 155(1-2):231–263, 2013.

[35] B Tirozzi and M Tsodyks. Chaos in highly diluted neural networks. *EPL (Europhysics Letters)*, 14(8):727–732, 1991.

[36] Lloyd N. Trefethen and Mark Embree. *Spectra and pseudospectra: the behavior of nonnormal matrices and operators*. Princeton University Press, 2005.

[37] Ekkehard Ullner, Antonio Politi, and Alessandro Torcini. Ubiquity of collective irregular dynamics in balanced networks of spiking neurons. *arXiv*, pages 1–5, 2017.

[38] Carl van Vreeswijk and Haim Sompolinsky. Chaotic balanced state in a model of cortical circuits. *Neural computation*, 10(6):1321–71, aug 1998.

[39] Tim P Vogels, H Sprekeler, F Zenke, C Clopath, and W Gerstner. Inhibitory plasticity balances excitation and inhibition in sensory pathways and memory networks. *Science (New York, N.Y.)*, 334(6062):1569–73, dec 2011.

[40] Maxim Volgushev, Sylvain Chauvette, and Igor Timofeev. Long-range correlation of the membrane potential in neocortical neurons during slow oscillation. *Progress in Brain Research*, 193:181–199, 2011.

# Supporting Information Legends

**Figure S1 (see Fig 3). Near Perfect Coherence as Strength of Structured Connectivity is Increased.** **(A)** Plot of coherence, $\chi$, vs strength of structured connectivity, $J_1$, for networks of size $N = 16000$ with row balance. Dots display average over realizations, bars display standard deviation. Only chaotic realizations included (those not found to be at a fixed point or a limit cycle - see methods). More than 20 realizations per value of $J_1$. For $J_1 = 100$, 22 out of 30 realizations were chaotic and the average coherence was 0.963.

**Figure S2 (see Fig 4). Real Leading Eigenvalues Yield Fixed Points.** **(A)** Sample chaotic dynamics for $J_1 = 0.1$. **(B)** Sample dynamics of same connectivity realization as in (A) but with $J_1 = 1$. **(C)** Scatterplot of all individual local-fields at fixed point, $h_i^*$, plotted against individual components of the leading eigenvector, $u_i^1$. Red dot is value of coherent mode at FP. Black dashed line is FP value predicted from theory. **(D)** Value of coherent mode of local-field at FP, $y^*$, as a function of the standard deviation of the random connectivity, $g$. Black line is prediction from theory: $y^* = \mathrm{sech}^{-1}\left(\frac{1}{\sqrt{g}}\right)$. $N = 4000$. Networks in all panels have row balance.

**Figure S3 (see Fig 4). Complex Leading Eigenvalues Yield Limit Cycles.** **(A)** Top: Sample chaotic dynamics for $J_1 = 0.25$. Bottom: Autocorrelation of coherent mode of local-field shows oscillatory ringing. **(B)** Same connectivity realization as (A) but with $J_1 = 2$. Dashed pink line in top panel is prediction from solving the three-dimensional dynamics. Autocorrelation shows near-perfect oscillations. **(C)** Projection of the full local-field dynamics of (B) onto coherent mode and the real and imaginary parts of the leading eigenvector. These three dimensions account for more than 0.99 of the total variance. Gray projection onto the leading eigenvector plane accounts for 0.98 of the variance of the residual local fields. **(D)** Scatterplot of period of oscillations plotted against the phase of the leading eigenvalue, $\frac{\mathrm{Im}\lambda_1}{\mathrm{Re}\lambda_1}$, of $\tilde{\mathbf{J}}$, for 219 different realizations of the random connectivity. Black line shows prediction from theory, $T = 2\pi\frac{\mathrm{Re}\lambda_1}{\mathrm{Im}\lambda_1}$. Networks in all panels have row balance.

**Figure S4. Coherent Dynamics and Switching Between Slow States With Non-symmetric Transfer Function.** **(A)** We use a non-symmetric transfer function $\phi(h) = (1 + \exp -\beta h)^{-p}$ with $\beta = 4$ and $p = \frac{1}{2}$. **(B)** Activity trace of coherent activity $\bar{\phi}(t)$ in black and 10 randomly chosen neurons $\phi_i(t)$ displays coherent switching between slow states. **(C)** Histogram of values of coherent current, $\bar{h}$, displays bimodality with peaks near the critical values predicted by theory where $\phi'\left(\bar{h}\right) = \frac{1}{g}$. Simulations for $N = 2000$ and $g = 2$ with row balance.